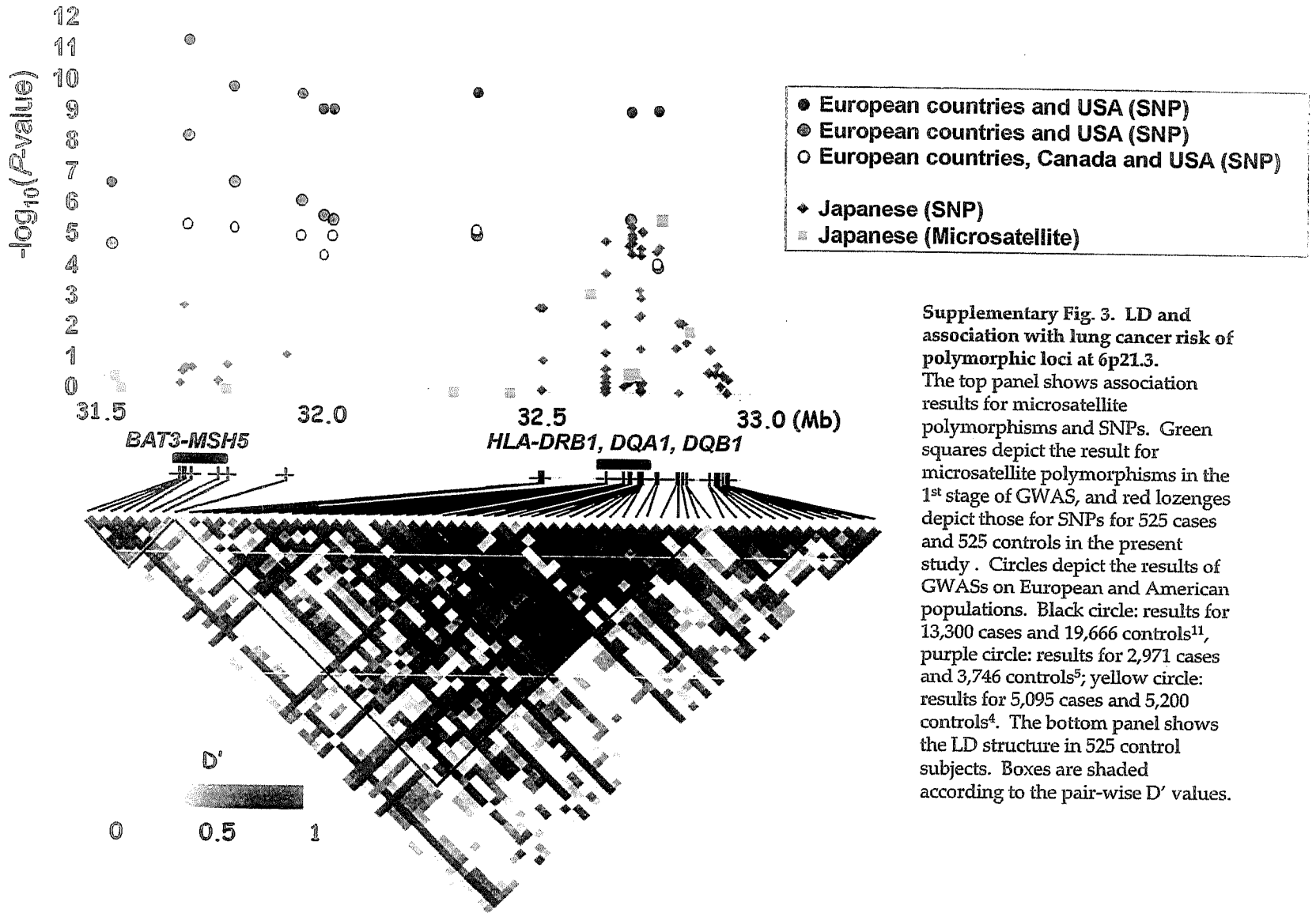

Supplementary Fig. 3. LD and association with lung cancer risk of polymorphic loci at 6p21.3.
The top panel shows association results for microsatellite polymorphisms and SNPs. Green squares depict the result for microsatellite polymorphisms in the 1st stage of GWAS, and red lozenges depict those for SNPs for 525 cases and 525 controls in the present study . Circles depict the results of GWASs on European and American populations. Black circle: results for 13,300 cases and 19,666 controls[11], purple circle: results for 2,971 cases and 3,746 controls[5]; yellow circle: results for 5,095 cases and 5,200 controls[4]. The bottom panel shows the LD structure in 525 control subjects. Boxes are shaded according to the pair-wise D' values.

INTERNAL MEDICINE

□ CASE REPORT □

Glucagonoma Diagnosed by Arterial Stimulation and Venous Sampling (ASVS)

Yukiyoshi Okauchi[1], Takao Nammo[1], Hiromi Iwahashi[1], Takashi Kizu[1], Isao Hayashi[1], Kohei Okita[1], Kazuya Yamagata[1], Sae Uno[1], Fumie Katsube[1], Munehide Matsuhisa[1], Ken Kato[1], Katsuyuki Aozasa[2], Tonsok Kim[3], Keigo Osuga[3], Shoji Nakamori[4], Yasuhiro Tamaki[5], Tohru Funahashi[1], Jun-ichiro Miyagawa[6] and Iichiro Shimomura[1]

Abstract

To identify the location of pancreatic endocrine tumors, arterial stimulation and venous sampling (ASVS) is known to be useful for insulinoma and gastrinoma, but its usefulness for glucagonoma has not been verified to date. Here we report a case of glucagonoma that was diagnosed by ASVS with calcium loading, in which an approximately 6-fold increase of glucagon was observed in the splenic artery territory. MEN1 gene analysis verified the presence of a mutation and the glucagonoma was confirmed after operation. In conclusion, ASVS could be useful for the diagnosis of glucagonoma.

Key words: multiple endocrine neoplasia type 1, arterial stimulation and venous sampling, glucagonoma

(Inter Med 48: 1025-1030, 2009)
(DOI: 10.2169/internalmedicine.48.1676)

Introduction

Multiple endocrine neoplasia type 1 (MEN1) is a multiple endocrine neoplasia complex in which hyperparathyroidism caused by parathyroid hyperplasia is associated with pancreatic endocrine tumors and pituitary adenomas. The causative gene is *MEN1*, which exhibits an autosomal dominant pattern of inheritance. Pancreatic endocrine tumors are found in approximately 65-75% of MEN1 patients (1). Regarding pancreatic endocrine tumors, pancreatic polypeptide (PP)-secreting tumors are the most common pancreatic endocrine tumor in MEN1 patients, occurring in 80% or more. They are usually accompanied by gastrinoma, while insulinoma, glucagonoma, and VIPoma are found in approximately 20%, 3%, and 1%, respectively (2). Among the pancreatic endocrine tumors that occur in MEN1 patients, glucagonoma is most often malignant and thus it requires early detection and early treatment.

However, locating these tumors is not always easy. Ultrasound, CT, and MRI are the commonly used diagnostic imaging methods for pancreatic endocrine tumors, while angiography is considered the most effective method (although more invasive) for detecting such tumors since these lesions are frequently hypervascular (3). Arterial stimulation and venous sampling (ASVS) is known to be useful for localizing insulinoma and gastrinoma, with a high detection sensitivity for insulinoma being reported (4-8), but its usefulness for detecting glucagonoma has not been determined. Here, we report a case of MEN1 in which glucagonoma was located by ASVS with calcium loading.

Case Report

The patient was a 66-year-old woman with no family history of endocrine tumors. She noticed a swelling in the right anterior cervical region at the age of 38 years, but left it untreated. At the age of 52, hypercalcemia, hypophosphatemia,

[1]Department of Metabolic Medicine, Graduate School of Medicine, Osaka University, Suita, [2]Department of Pathology, Graduate School of Medicine, Osaka University, Suita, [3]Department of Radiology, Graduate School of Medicine, Osaka University, Suita, [4]Department of Surgery, Osaka National Hospital, Osaka, [5]Department of Breast and Endocrine Surgery, Graduate School of Medicine, Osaka University, Suita and [6]Department of Internal Medicine, Division of Diabetes and Metabolism, Hyogo College of Medicine, Nishinomiya
Received for publication September 8, 2008; Accepted for publication March 13, 2009
Correspondence to Dr. Yukiyoshi Okauchi, okauchi@imed2.med.osaka-u.ac.jp

Table 1. Laboratory Tests on Admission

RBC	431×10^4/μL	Cr	1.2 mg/dL
Hb	13.8 g/dL	BUN	26 mg/dL
WBC	6560/μL	UA	5.7 mg/dL
Plt	18.7×10^4/μL	Na	144 mEq/L
FPG	107 mg/dL	K	4.1 mEq/L
HbA1c	6.6 %	Cl	112 mEq/L
IRI	20 μU/mL	Ca	5.2 mEq/L
CPR	5.5 ng/mL	P	2.4 mEq/L
T-chol	202 mg/dL	CRP	<0.2 mg/dL
TG	191 mg/dL		
HDL-C	80 mg/dL	Urinalysis	
LDL-C	163.8 mg/dL	pH	7.0
TP	6.6 g/dL	Protein	(+/-)
Alb	3.9 g/dL	Sugar	(-)
T-Bil	0.4 mg/dL	Occult	(-)
AST	13 U/L	Acetone	(-)
ALT	9 U/L	Ccr	29.9 mL/min
γ-GTP	32 U/L	Alb	29.6 mg/day
ALP	118 U/L	CPR	137.7 μg/day
LDH	248 U/L		

and high plasma PTH levels were detected by a local clinic, and the patient visited our hospital the following year. Hyperparathyroidism was detected and subtotal parathyroidectomy (leaving 1/2 of the upper left gland) was performed. At that time, MEN1 was suspected. Endocrinology investigations and imaging studies were performed, but no additional abnormality was found, except for PTH levels. After surgery, her Ca and PTH levels decreased, and the patient was discharged. From the age of 54 years, the patient began to experience backache and bone pain, and her Ca and PTH levels became slightly elevated. At the age of 58, the 75 g OGTT was performed when the patient was admitted for investigation of her back pain, and it demonstrated a diabetic pattern. Her bone pain continued to worsen, and the patient was followed up by a local clinic. When the patient revisited our hospital at the age of 66 years, ultrasound revealed a 10×8×4 mm low echoic lesion in the dorsal part of the left lobe of the thyroid gland, and a high-intensity area was also seen on T2-weighted MR images. Blood tests revealed the following abnormal findings: Ca was 5.2 mEq/L, P was 2.6 mEq/L, and PTH was 99.0 pg/mL. The patient was admitted to our hospital in the same year for investigation and treatment.

She was 153 cm tall and weighed 52.8 kg. Blood pressure was 118/60 mmHg. Physical examination revealed degradation of vibratory sensation of inferior limbs and numbness of upper and lower limbs. She had high Ca and PTH levels, a low P level, and impaired renal function (Table 1). ^{99}mTc-MIBI scintigraphy revealed an area of increased uptake in the parathyroid behind the left lobe of the thyroid gland. Since her serum levels of Ca and PTH were persistently elevated and renal dysfunction was observed, we considered a good indication for surgery. Endocrine studies (Table 2) revealed elevation of pancreatic endocrine hormones and abdominal imaging showed nodules (5 mm and 25 mm in diameter) in the tail of the pancreas, suggesting the presence of pancreatic islet tumors (Fig. 1). Treatment of her hyperparathyroidism was given priority, and the patient was transferred to the Department of Endocrine Surgery for removal of the remaining parathyroid gland. Pathologic examination of the resected gland revealed hyperplasia, but no obvious malignancy. The PTH level was 157.5 pg/mL prior to surgery, and it fell to 55.1 pg/mL at 15 minutes after removal of the gland. The resected parathyroid gland measured 10×9 mm. Part of the gland was autotransplanted into the left forearm after it had been cut into small pieces. Her serum calcium level improved to 4.8 mEq/L after surgery. The patient was subsequently transferred to our department for further testing because MEN1 was suspected.

Plain MRI of the head did not reveal any findings suggestive of pituitary adenoma. Although the basal level of GH was high, the 75 g OGTT caused inhibition of GH secretion, ruling out the possibility of GHoma. Plain CT of the abdomen revealed a low-density mass (5 mm in diameter) in the right adrenal gland, suggesting the presence of an adenoma. Adrenocortical and adrenomedullary hormones study showed elevated renin and aldosterone levels, but the serum and urinary levels of cortisol, adrenalin, and noradrenalin were all within the normal range or only slightly elevated. Combined with the fact that suppression of cortisol was noted in the rapid dexamethasone suppression test, the mass was concluded to be a non-functioning adrenal tumor. Her pancreatic endocrine tumor was initially suspected to be an insulinoma based on the elevated levels of IRI and CPR. When a CPR suppression test and euglycemic/hypoglycemic clamp tests were performed, suppression of CPR was insufficient. Then we planned ASVS to make a diagnosis and localize the insulinoma. In addition, because our institution had made diagnosis for glucagonoma using ASVS before (9), we planned to rule out the possibility of glucogonoma. ASVS was performed according to procedures described previously (4), and we used the criteria reported by Hayashi et al (10). We used Calcicol® (Dainippon-Sumitomo Co. Ltd., Osaka, Japan) in this case as the calcium gluconate 8.5%. Calcicol® was injected as a bolus at a dose of 0.025 mEq Ca^{2+}/kg body weight into each selective catheterized artery. When ASVS was performed, a selective increase of insulin was not detected, but an approximately 6-fold increase of glucagon was observed in the splenic artery territory, strongly suggesting the presence of a glucagonoma (Fig. 2). Thus, diagnostic imaging revealed multiple tumors in the pancreas ranging from 5 to 25 mm in diameter, and there was elevation of the basal levels of insulin, glucagon, somatostatin, and pancreatic polypeptide (PP). In addition, ASVS demonstrated elevation of glucagon in the splenic artery territory, which includes the tail of the pancreas. Based on these findings, a diagnosis of glucagonoma was suspected and laparoscopic distal pancreatectomy was performed. The resected tail of the pancreas contained tumors measuring 5 mm and 20 mm in diameter, corresponding to the lesions identified by imaging studies (Fig. 3). Partial hepatectomy was also performed because white nodules, sev-

Table 2. **Hormonal Examinations of the Present Patient**

	on admission	post operation	post Op 6 months	normal range
GH	6.3 ng/mL		3.7 ng/mL	< 6.0 ng/mL
IGF-1	414 ng/mL			121-436 ng/mL
ACTH	38.0 pg/mL		29 pg/mL	< 60 pg/mL
PRL	16.9 ng/mL		12.0 ng/mL	< 27 ng/mL
LH	22.3 mIU/mL		39.4 mIU/mL	4.2-79.6 mIU/mL
FSH	84.3 mIU/mL		112.6 mIU/mL	12.6-235.7 mIU/mL
TSH	2.84 μIU/mL		4.38 μIU/mL	0.40-3.80 μIU/mL
FT4	1.1 ng/dL		1.0 ng/dL	1.0-1.6 ng/dL
FT3	2.2 pg/mL		2.4 pg/mL	2.1-3.8 pg/mL
PTH	113 pg/mL	62 pg/mL	111 pg/mL	14-66 pg/mL
calcitonin	77.0 pg/mL		42 pg/mL	21.6-54.0 pg/mL
IR-glucagon	271 pg/mL	194 pg/mL	214 pg/mL	40-140 pg/mL
FPG	107 mg/dL	110 mg/dL	140 mg/dL	70-110 mg/dL
IRI	20 μU/mL	10 μU/mL	6 μU/mL	< 12 μU/mL
CPR	5.5 ng/mL	3.0 ng/mL	2.4 ng/mL	1.0-2.0 ng/mL
PP	847 pg/mL			< 326 pg/mL
gastrin	93.0 pg/mL			30-150 pg/mL
somatostatin	18.0 pg/mL			1.0-12.0 pg/mL
cortisol	25.2 μg/dL		14.9 μg/dL	4.5-24.0 μg/dL
urinary cortisol	20.1 μg/day			35-160 μg/day
renin activity	4.2 ng/mL/hr		12.1 ng/mL/hr	0.2-2.7 ng/mL/hr
aldosterone	19.7 ng/dL		12.1 ng/dL	2.0-13.0 ng/dL
adrenaline	0.02 ng/mL		0.02 ng/mL	< 0.17 ng/mL
noradorenaline	0.35 ng/mL		0.38 ng/mL	0.15-0.52 ng/mL

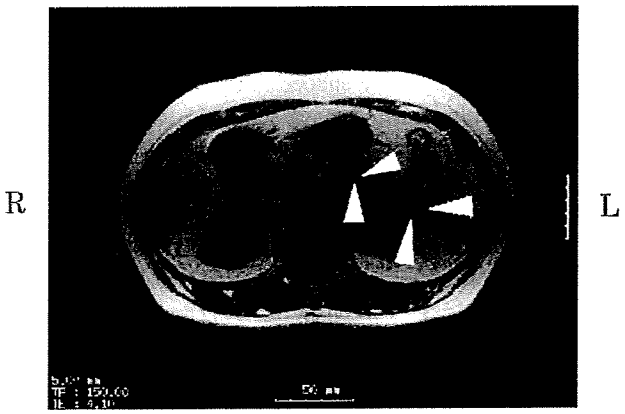

Figure 1. Abdominal MR imaging showed nodules in the pancreas (diameter 5 mm in body [center arrowhead], 25 mm in tail [end arrowhead]), suggesting the presence of pancreatic islet tumors.

eral millimeters in size, were found on the surface of the left lobe of the liver during surgery. The resected pancreatic tumors were determined to be islet cell tumors by pathologic examination. Both tumors were composed of cells with trabecular or ribbon-like proliferation, and were encapsulated with no signs of invasion into the surrounding tissue. Immunostaining revealed numerous glucagon-positive cells, as well as some cells that were positive for insulin, somatostatin, or PP in both tumors (Fig. 4a-d). On pathological examination, the white nodules on the surface of the left lobe of the liver were shown to be regions of fibrosis and lipidosis, ruling out the possibility of liver metastasis. When endocrine studies were performed three weeks after surgery, the levels of pancreatic endocrine hormones were lower (glucagon was 194 pg/mL, IRI was 10 μU/mL, CPR was 3.0 ng/mL, and somatostatin was 14 pg/mL) than before the operation. In addition, we examined MEN1 gene, after written informed consent was obtained from the patient, and c.734 delC was found at exon 4 (Fig. 5).

Discussion

Glucagonoma was first reported in 1966 by McGavran et al (11). The abnormal production of glucagon leads to a diabetic state and hypoaminoacidemia, along with symptoms such as weight loss, impaired glucose tolerance, skin rashes, mouth ulcers, and anemia. Mallinson et al referred to these symptoms as the glucagonoma syndrome (12). In the pres-

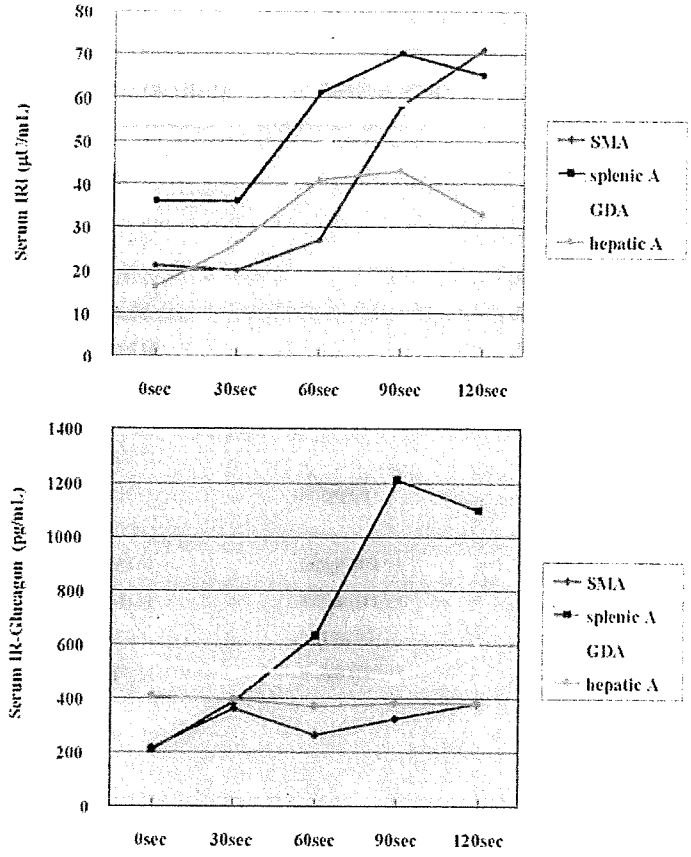

Figure 2. **Results of arterial stimulation and venous sampling (ASVS) in the present case. Each line represents insulin and glucagon levels in the hepatic vein after injection of calcium gluconate 8.5% was injected as a bolus at a dose of 0.025 mEq Ca^{2+}/kg body weight into the gastroduodenal artery (GDA), superior mesenteric artery (SMA), splenic artery (SA), and hepatic artery (HA). A selective increase of insulin was not detected, but an approximately 6-fold increase of glucagon was observed in the splenic artery territory.**

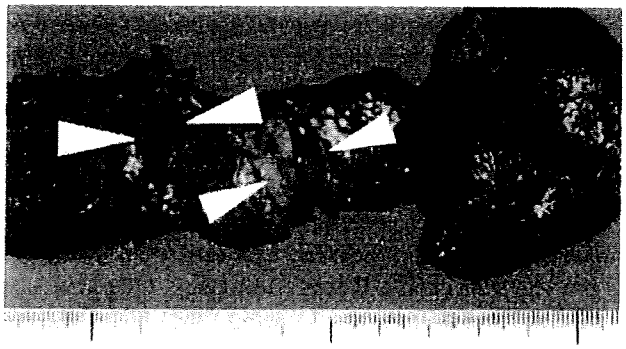

Figure 3. **Macroscopic findings of the tumor. The resected tail of the pancreas contained tumors measuring 5 mm and 20 mm in diameter, corresponding to the lesions identified by imaging studies.**

ent patient, recurrence of hypercalcemia and parathyroid hyperplasia were noted while the patient was being followed up after subtotal parathyroidectomy performed 13 years earlier. Further investigation revealed the presence of pancreatic endocrine tumors and an adrenal tumor, leading to the diagnosis of MEN1. Since pancreatic islet tumors are found in 65-75% of MEN1 patients and glucagonoma is frequently malignant among these endocrine tumors of the pancreas, a differential diagnosis of pancreatic endocrine tumors is vital to facilitate early detection and early treatment. The presence of liver metastasis is considered to be the chief prognostic factor for glucagonoma. In the present case, nodules were found on the left lobe of the liver during distal pancreatectomy, but metastasis was ruled out by pathologic examination. In addition, two endocrine pancreas tumors were detected in the present case and we examined the malignancy of each tumor using Ki-67 index. We examined Ki-67 index, using a method previously reported (13), and found that the Ki-67 index was quite low. Thus the possibility of malignancy of both tumors was thought to be low (13). Nevertheless, the patient will need to be followed up with periodic imaging studies. The value of provocative tests using secretagogues for diagnosing and locating endocrine tumors is well known. Imamura and Doppman et al performed selective arterial infusion of stimulants to locate an endocrine tumor by identification of the feeding artery, and reported that gastrinoma and insulinoma could be localized by loading tests with secretin and calcium, respectively (4-8), but the

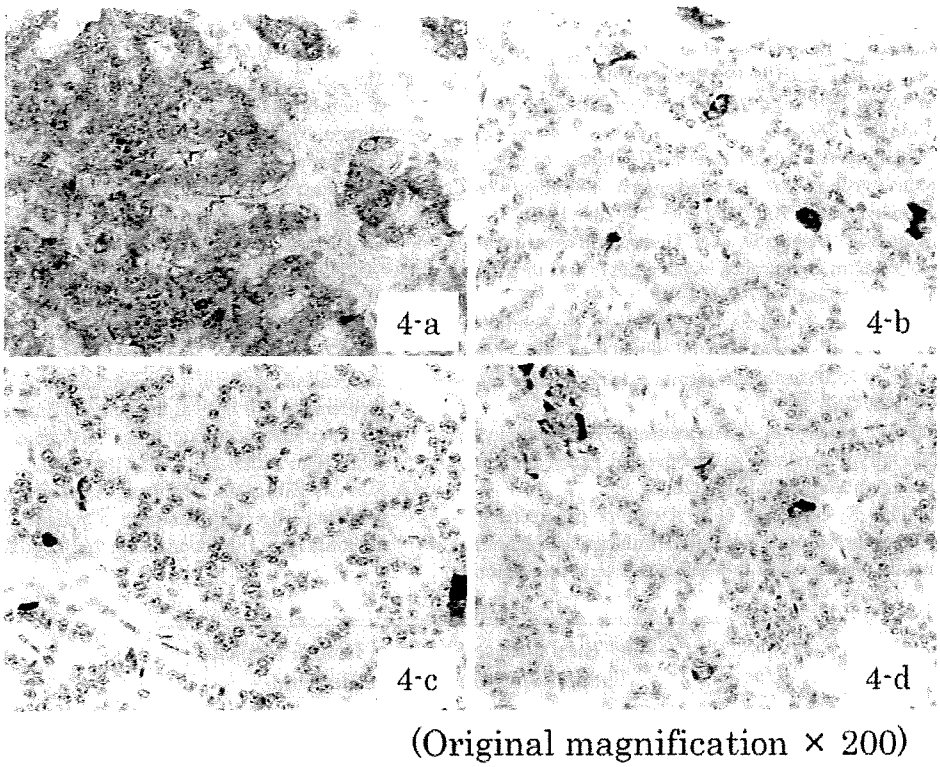

Figure 4. **Microscopic findings of the tumor (20 mm in diameter) (×200). Immunohistochemical staining for glucagon (4-a), insulin- (4-b), somatostatin- (4-c), or pancreatic polypeptide (PP) (4-d). Immunohistostaining revealed numerous glucagon-positive cells, as well as some cells that were positive for insulin-, somatostatin-, or PP.**

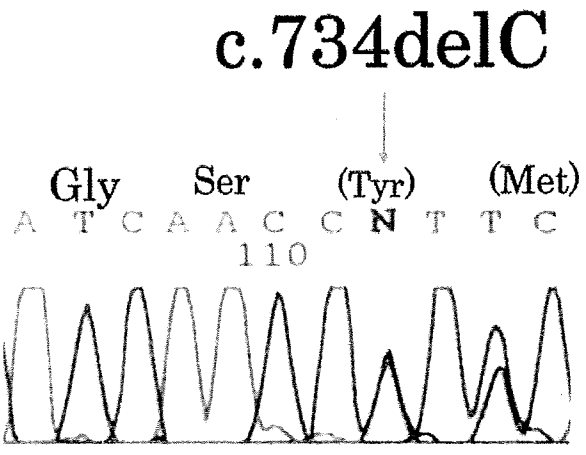

Figure 5. **DNA sequence of MEN1 gene was examined in this patient. c.734delC was found at exon 4.**

use of ASVS for glucagonoma has not been reported except for one case at our hospital (9). In the present case, the fasting glucagon level was 271 pg/mL (not extremely high) and skin symptoms were lacking. In addition, the patient had long-standing impaired glucose tolerance, which made secondary hyperglucagonemia and hyperinsulinemia possibility. Thus, the diagnosis of glucagonoma was difficult from only the basal values of hormones. However, ASVS revealed elevation of the glucagon level in the splenic artery territory, while insulin did not show a response suggestive of insulinoma. Our experience suggests that ASVS with calcium loading is a useful test for glucagonoma, particularly for preoperative diagnosis in patients with only a slight elevation of basal glucagon values. When the causative gene was examined in the patient, c.734delC was found at exon 4. This was the same mutation that Sato et al reported as 842 delC in 2000 (14).

Acknowledgement

We thank all members of medical staff in the Department of Metabolic Medicine and Department of Gastroenterological Surgery, Osaka University Hospital for their valuable help with this work.

References

1. Bartsch DK, Fendrich V, Langer P, Celik I, Kann PH, Rothmund M. Outcome of duodenopancreatic resections in patients with multiple endocrine neoplasia type 1. Ann Surg **242**: 757-766, 2005.
2. Doherty GM. Multiple endocrine neoplasia Type 1. J Surg Oncol **89**: 143-150, 2005.
3. Doi R, Komoto I, Nakamura Y, et al. Pancreatic endocrine tumor

in Japan. Pancreas **28**: 247-252, 2004.

4. Doppman JL, Chang R, Fraker DL, et al. Localization of insulinomas to regions of the pancreas by intra-arterial stimulation with calcium. Ann Intern Med **123**: 269-273, 1995 (Erratum in: Ann Intern Med **123**: 734, 1995).
5. Imamura M, Takahashi K, Adachi H, et al. Usefulness of selective arterial secretin injection test for gastrinoma in patients with Zollinger-Ellison syndrome. Ann Surg **205**: 230-239, 1987.
6. Imamura M, Hattori Y, Nishida O, et al. Unresponsiveness of insulinoma cells to secretin: significance of the secretin test in patients with insulinoma. Pancreas **5**: 467-473, 1990.
7. Brandle M, Pfammatter T, Spinas GA, Lehmann R, Schmid C. Assessment of selective arterial calcium stimulation and hepatic venous sampling to localize insulin-secreting tumors. Clin Endocrinol (Oxf) **55**: 357-362, 2001.
8. Tonelli F, Fratini G, Nesi G, et al. Pancreatectomy in multiple endocrine neoplasia Type 1-related gastrinoma and pancreatic endocrine neoplasias. Ann Surg **244**: 61-70, 2006.
9. Yoshio N, Kitajima K, Ohsato H, et al. A case of pancreatic glucagonoma of diameter 15 mm, discovered with medical examination and a calcium tolerance test in a selective artery was effective in preoperative diagnosis. Hormon To Rinsho (Clinical Endocrinology) **46**: S156-S161, 1998 (in Japanese).
10. Hayashi T, Honda H, Yasumori K, et al. Selective intra-arterial injection of calcium for localization of insulinomas: proposed new criteria. Nippon Igaku Hoshasen Gakkai Zasshi **55**: 952-956, 1995 (in Japanese, Abstract in English).
11. McGavran MH, Unger RH, Recant L, Polk HC, Kilo C, Levin ME. A glucagon-secreting alpha-cell carcinoma of the pancreas. N Engl J Med **274**: 1408-1413, 1966.
12. Mallinson CN, Bloom SR, Warin AP, Salmon PR, Cox B. A glucagonoma syndrome. Lancet **2**: 1-5, 1974.
13. Pelosi G, Bresaola ME, Bogina CG, et al. Endocrine tumors of the pancreas: Ki-67 immunoreactivity on paraffin sections is an independent predictor for malignancy: A comparative study with proliferating-cell nuclear antigen and progesterone receptor protein immunostaining, mitotic index, and other clinicopathologic variables. Hum Pathol **27**: 1124-1134, 1996.
14. Sato M, Kihara M, Nishitani A, et al. Large and asymptomatic pancreatic islet cell tumor in a patient with multiple endocrine neoplasia type 1. Endocrine **13**: 263-266, 2000.

THE JOURNAL OF BIOLOGICAL CHEMISTRY VOL. 284, NO. 42, pp. 29041–29049, October 16, 2009

Prolyl 4-Hydroxylation of α-Fibrinogen

A NOVEL PROTEIN MODIFICATION REVEALED BY PLASMA PROTEOMICS[*S]

Received for publication, July 6, 2009, and in revised form, August 18, 2009 Published, JBC Papers in Press, August 20, 2009, DOI 10.1074/jbc.M109.041749

Masaya Ono,[a1] Junichi Matsubara,[a] Kazufumi Honda,[a] Tomohiro Sakuma,[b] Tomoyo Hashiguchi,[c] Hiroshi Nose,[c] Shoji Nakamori,[d] Takuji Okusaka,[e] Tomoo Kosuge,[f] Naohiro Sata,[g] Hideo Nagai,[g] Tatsuya Ioka,[h] Sachiko Tanaka,[h] Akihiko Tsuchida,[i] Tatsuya Aoki,[i] Masashi Shimahara,[j] Yohichi Yasunami,[k] Takao Itoi,[l] Fuminori Moriyasu,[l] Ayako Negishi,[a] Hideya Kuwabara,[b] Ayako Shoji,[b] Setsuo Hirohashi,[a] and Tesshi Yamada[a,l]

From the [a]Chemotherapy Division, National Cancer Center Research Institute, the [e]Pancreatic Oncology Division, and the [f]Hepatobiliary and Pancreatic Surgery Division, National Cancer Center Hospital, 5-1-1 Tsukiji, Chuo-ku, Tokyo 104-0045, the [b]Bioscience Team, Consulting Business Unit, Mitsui Knowledge Industry, 2-5-1 Atago, Minato-ku, Tokyo 105-6215, the [c]Kobe Research Center, Transgenic Inc., 7-1-14 Minatojimaminami-machi, Chuo-ku, Kobe 650-0047, the [d]Department of Surgery, Osaka National Hospital, 2-1-14 Hoenzaka, Chuo-ku, Osaka 540-0006, the [g]Department of Surgery, Jichi Medical School, 3311-1 Yakushiji, Minamikawachi, Tochigi 329-0498, the [h]Department of Hepatobiliary and Pancreatic Oncology, Osaka Medical Center for Cancer and Cardiovascular Diseases, 1-3-3 Nakamichi, Higashinari, Osaka 537-8511, the [i]Third Department of Surgery and [l]Fourth Department of Internal Medicine, Tokyo Medical University, 6-7-1 Nishi-Shinjuku, Shinjuku-ku, Tokyo 160-0023, the [j]Department of Oral Surgery, Osaka Medical College, 2-7 Daigaku-machi, Takatsuki-Shi, Osaka 569-8686, and the [k]Department of Regenerative Medicine and Transplantation, Fukuoka University Faculty of Medicine, 7-45-1 Nanakuma, Jonan-ku, Fukuoka 814-0180, Japan

Plasma proteome analysis requires sufficient power to compare numerous samples and detect changes in protein modification, because the protein content of human samples varies significantly among individuals, and many plasma proteins undergo changes in the bloodstream. A label-free proteomics platform developed in our laboratory, termed "Two-Dimensional Image Converted Analysis of Liquid chromatography and mass spectrometry (2DICAL)," is capable of these tasks. Here, we describe successful detection of novel prolyl hydroxylation of α-fibrinogen using 2DICAL, based on comparison of plasma samples of 38 pancreatic cancer patients and 39 healthy subjects. Using a newly generated monoclonal antibody 11A5, we confirmed the increase in prolyl-hydroxylated α-fibrinogen plasma levels and identified prolyl 4-hydroxylase A1 as a key enzyme for the modification. Competitive enzyme-linked immunosorbent assay of 685 blood samples revealed dynamic changes in prolyl-hydroxylated α-fibrinogen plasma level depending on clinical status. Prolyl-hydroxylated α-fibrinogen is presumably controlled by multiple biological mechanisms, which remain to be clarified in future studies.

For comprehensive analysis of plasma proteins, it is necessary to compare a sufficient number of blood samples to avoid simple interindividual heterogeneity, because the protein content of human samples varies significantly among individuals. Also, the provision of sufficient power is needed to detect protein modification because many plasma proteins undergo changes in the bloodstream (1). Even though the proteomic technologies have advanced (2, 3), there remains room for improvement. Different isotope labeling and identification-based methods have been developed for quantitative proteomics technologies (4–6), but the number of samples that can be compared by the current isotope-labeling methods is limited, and identification-based proteomics is unable to capture information regarding unknown modifications.

A label-free proteomics platform developed in our laboratory, termed "Two-Dimensional Image Converted Analysis of Liquid chromatography and mass spectrometry (2DICAL)[2] (7), simply compares the liquid chromatography and mass spectrometry (LC-MS) data and detects a protein modification by finding changes in the mass to charge ratio (m/z) and retention time (RT). Enhanced methods for accurate MS peak alignment across multiple LC runs have enabled the successful implementation of clinical studies requiring comparison of a large number of samples (8, 9). Using 2DICAL to analyze plasma samples of pancreatic cancer patients and healthy controls, novel prolyl hydroxylation of α-fibrinogen was successfully discovered.

Fibrinogen and its modification has been investigated because of its clinical importance (10, 11). On the other hand, prolyl hydroxylation has attracted attention after the discovery of the hypoxia-inducible factor 1α (HIF1α) prolyl-hydroxylase and its role in switching of HIF1α functions (12). Prolyl hydroxylation in other proteins has been energetically sought,

* This work was supported by the Program for Promotion of Fundamental Studies in Health Sciences conducted by the National Institute of Biomedical Innovation of Japan and by the Third-Term Comprehensive Control Research for Cancer conducted by the Ministry of Health, Labor and Welfare of Japan.

[S] The on-line version of this article (available at http://www.jbc.org) contains supplemental Figs. S1–S7 and Tables S1–S3.

[1] To whom correspondence should be addressed. Fax: 81-3-3547-5298; E-mail: masono@ncc.go.jp.

[2] The abbreviations used are: 2DICAL, two-dimensional image converted analysis of liquid chromatography and mass spectrometry; CC, correlation coefficient; Con A, concanavalin A; CV, coefficient of variance; ELISA, enzyme-linked immunosorbent assay; ESI, electrospray; αFG, fibrinogen α-chain; GANP, germinal center-associated nuclear protein; HIF1, hypoxia-inducible factor-1; HyP, hydroxyproline; MS, mass spectrometry; MS/MS, tandem mass spectrometry; m/z, mass-to-charge ratio; OPD, orthophenylenediamine; P4H, prolyl 4-hydroxylase; QTOF, quadrupole time-of-flight; RT, retention time; siRNA, small interfering RNA.

but only a few such proteins have been identified (13). Only one study has reported prolyl hydroxylation of fibrinogen at the β chain (14).

Here, we report the detection of prolyl 4-hydroxylated α-fibrinogen by plasma proteome analysis, a protein modification that dynamically changes in plasma depending on the clinical status and is a candidate plasma biomarker.

EXPERIMENTAL PROCEDURES

Clinical Samples—Seventy-seven plasma samples (38 patients with pancreatic ductal adenocarcinoma and 39 healthy controls) were obtained from the National Cancer Center Hospital (Tokyo, Japan) (Sets 1 and 2), and 9 plasma samples (5 patients with pancreatic ductal adenocarcinoma and 4 healthy controls) were obtained from the Tokyo Medical University Hospital (Tokyo, Japan) (Set 3) (15). 685 plasma samples from patients with various diseases and healthy controls (Sets 4) were collected prospectively from seven medical institutions associated with the "Third-Term Comprehensive Control Research for Cancer" and will be described in detail elsewhere.[3] Written informed consent was obtained from every subject. The study was reviewed and approved by the ethics committee of each institute.

Sample Preparation—To 20 μl of a plasma sample, 900 μl of phosphate-buffered saline and 100 μl of Con A-agarose (Vector, Burlingame, CA) were added, and the sample was incubated at 4 °C for 2 h. After extensive washing with phosphate-buffered saline, proteins bound to Con A were eluted by competition with 100 mM mannose. To 30 μl of the eluted sample, 10 μl of 5 M urea, 2.5 μl of 1 M NH_4HCO_3, and 3.3 μg of sequencing grade modified trypsin (Promega, Madison, WI) were added. After digestion at 37 °C for 20 h, peptides were dried with a SpeedVac concentrator (Thermo Electron, Holbrook, NY) and then dissolved in 50 μl of 0.1% formic acid.

LC-MS—LC-MS and data acquisition were performed as reported previously (7, 8). Briefly, the peptide samples were separated with a linear gradient from 0 to 80% acetonitrile in 0.1% formic acid at a flow rate of 200 nl/min for 60 min using the splitless nano-flow HPLC systems (DiNa (KYA, Tokyo, Japan)) (16). MS spectra were acquired every second in triplicate with nano-electrospray (nanoESI)-QTOF-MS (QTOF Ultima (Waters, Milford, MA)).

Peak Alignment Across Multiple LC-MS—MS peaks were detected, normalized, and quantified using the in-house 2DICAL software package, as described previously (7). To increase the accuracy of peak alignment across multiple LC-MS runs, we applied a greedy algorithm, which had been used for fast DNA sequence alignment, to supplement our previous method (8, 9).

Protein and Modification Identification—MS and MS/MS data were acquired by preparative LC-MS runs with a tolerance of ±0.1 *m/z* and ± 0.5 min of RT using QTOF Ultima and linear ion trap (LTQ)-Orbitrap (Thermo Fisher Scientific, Waltham, MA) mass spectrometers. The MS/MS data were analyzed with Mascot software (Matrix Sciences, London, UK) including oxidized histidine, oxidized methionine, and hydroxyproline as possible modifications. Chemical formulas were determined with Xcalibur software (Thermo Fisher Scientific) with mass tolerance of 5 ppm.

Cell Lines—Primary cultured normal hepatic cells (hNHeps) were purchased from Takara Bio (Shiga, Japan). KIM-1 was kindly provided by Dr. Masamichi Kojiro (Kurume University, Kurume, Japan). Hep3B was obtained from the Cell Resource Center for Biomedical Research, Tohoku University (Sendai, Japan). HLE was obtained from the Health Science Research Resources Bank (Osaka, Japan). SK-Hep-1, Jhh-7, Hep-G2, HuH-7, and HuH-6clone5 were purchased from the American Type Culture Collection (ATCC, Manassas, VA).

RNA Interference—Three siRNAs targeting each of the *P4HA1*, *P4HA2*, *P4HA3*, *P4HB*, *EGNL1*, *EGNL2*, and *EGNL3* genes, as well as 2 control RNAs, were designed by Applied Biosystems (Foster City, CA). Cells were transfected with the Lipofectamine 2000 reagent (Invitrogen, Carlsbad, CA) (17). Knockdown of relevant mRNA expression was confirmed by real-time PCR at 24 h after transfection (16).

Antibodies—Anti-fibrinogen antibody (A0080) was purchased from DAKO (Glostrup, Denmark). GANP transgenic mice (18) were immunized with a synthetic peptide ESSSHHP-(O)GIAEFPSR (P(O), hydroxyproline) (named HyP-ESS) conjugated to keyhole limpet hemocyanin. Monoclonal antibodies were generated by a standard cell fusion technique. The reactivity and titer of antibodies to HyP-ESS as well as unmodified (ESS) peptides were assessed by an antibody capture assay (19) using OPD (orthophenylenediamine) as a substrate (supplemental Fig. S6*A*).

Immunoblotting—Protein samples were separated by SDS-PAGE and electroblotted onto polyvinylidene difluoride membranes (Millipore, Billerica, MA). Blots were visualized with an enhanced chemiluminescence kit (GE Healthcare, Bucks, UK) and quantified as described previously (20).

Competitive ELISA—100 μl of plasma diluted 20-fold with phosphate-buffered saline or 100 μl of serially diluted HyP-ESS standard peptide were incubated with 100 μl of 1 μg/ml horseradish peroxidase-conjugated 11A5 antibody for 30 min. 50 μl of the solution was added to 96-well microtiter plates precoated with 50 ng of HyP-ESS peptide and incubated for 1 h. After extensive washing, wells were incubating with the OPD solution for 10 min, and color absorbance at 490 nm was measured (supplemental Fig. S6*D*).

Statistical Analyses—Mann-Whitney *U* test was performed with the open-source statistical language R (version 2.7.0) (9).

RESULTS

Large Scale Quantitative Plasma Proteomics of Pancreatic Cancer Patients—77 plasma samples (39 from patients with pancreatic cancer and 38 from healthy controls) were obtained from National Cancer Center Hospital. We used concanavalin A (Con A) to concentrate plasma glycoproteins (21). This "glycocapturing" procedure removed albumin and reduced the concentration of other abundant plasma proteins (22). Various aberrations of protein glycosylation accumulate in cancer (23,

[3] K. Honda, T. Okusaka, K. Felix, T. Umaki, M. Ono, S. Nakamori, N. Sata, H. Nagai, T. Ioka, S. Tanaka, A. Tsuchida, T. Aoki, T. Shimahara, M. Shimahara, Y. Yasunami, H. Kuwabara, Y. Otsuka, N. Ota, C. Ebihara, T. Kosuge, S. Hirohashi, M. W. Büchler, and T. Yamada, manuscript in preparation.

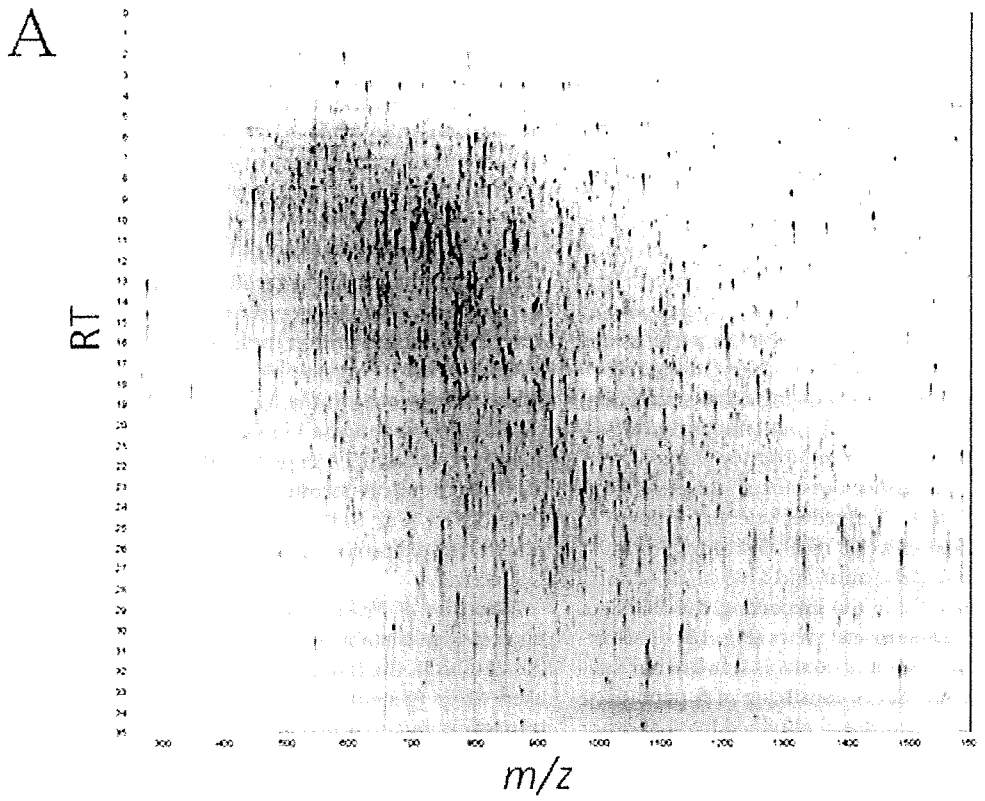

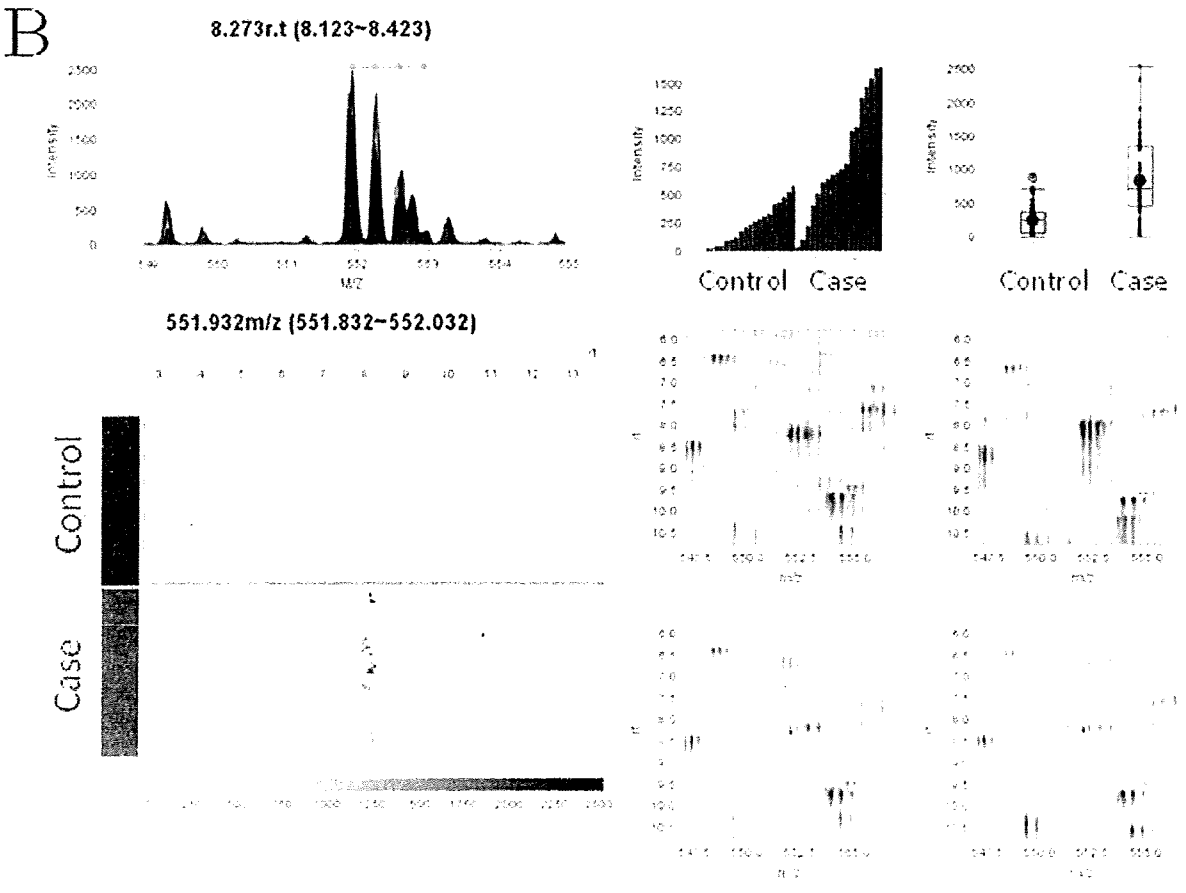

24). Most tumor markers of pancreatic cancer used clinically, including CA19-9, DUPAN-2, and NCC-ST-439, are known to be carbohydrate antigens (23, 25). Each sample was anonymized, randomized, and measured in triplicate by 2DICAL. A total of 115,325 independent MS peaks were detected within mass ranges of 250–1600 *m/z* and an LC RT of 0–45 min (Fig. 1*A*). The correlation coefficient (CC) and coefficient of variance (CV) values for the triplicate data were over 0.95 and under 0.15, respectively, in most subjects. To increase statistical robustness, 77 samples were separated at random into two experimental sets (Set 1 (18 pancreatic cancer patients and 19 healthy controls) and Set 2 (20 pancreatic cancer patients and 20 healthy controls)), and the two sets were analyzed independently. We selected 10 peptide peaks showing a statistically significant difference between the cancer patients and controls (>2 fold difference, $p < 0.0005$ (Mann-Whitney *U* test), average peak intensity of >10 in either the cancer samples or the control samples) in both sets. We further selected 6 peaks of 412 *m/z* (RT 13.7 min), 546 *m/z* (8.3 min), 552 *m/z* (8.3 min), 827 *m/z* (8.3 min), 1141 *m/z* (29.0 min), and 1185 *m/z* (9.2 min) (supplemental Fig. S1 and Table S1) inspecting the 2DICAL reports with various two-dimensional views (Fig. 1*B*). The difference between cancer patients and controls was further validated in an independent set (Set 3, consisting of 5 pancreatic cancer patients and 4 healthy controls) obtained from another medical institution (Tokyo Medical University Hospital) (supplemental Fig. S2).

Target MS/MS Analysis for Peak Identification—Target MS/MS data were acquired from preparative LC-MS. The MS/MS spectra of the peaks of 552 *m/z* and 827 *m/z* matched the same ESSSHHP*GIAEFPSR sequence of fibrinogen α-polypeptide isoform α-E preproprotein (NP_000499/NP_068657) with the highest Mascot scores (supplemental Fig. S3 and not shown; * indicates a mismatch (described below)). These peaks were considered to be differently charged masses (triply and doubly charged, respectively) derived from the same peptide. The triple-charged 546 *m/z* peak is considered to be a mass with neutral loss of H_2O, because its appearance was almost identical to the peaks of 552 and 827 *m/z*. The peak of 1141 *m/z* matched another peptide sequence of fibrinogen α-polypeptide isoform α-E preproprotein TFP*GFFSPMLGEFVSETESR with the highest Mascot score (supplemental Fig. S4). No significant match was found with the 412 *m/z* peak despite its highly qualified MS/MS spectrum (data not shown), probably because of an unknown post-translational modification, a non-annotated gene sequence (26), or proteolysis. Qualified MS/MS spectra were not obtained from the peak of 1185 *m/z*. We noticed 16-dalton smaller MS peaks at different locations (547 *m/z* (8.5 min), 819 *m/z* (8.6 min), and 1133 *m/z* (30.0 min)) that completely matched the same amino acid sequences of fibrinogen α-polypeptide as the peaks of 552 *m/z* (8.3 min), 827 *m/z* (8.3 min), and 1141 *m/z* (29.0 min), respectively (Fig. 2 and data not shown). However, the intensity of the three 16-dalton-smaller MS peaks did not differ significantly between pancreatic cancer patients and controls (Fig. 2*B*).

Determination of the 16-Dalton Increase by High Resolution MS—To clarify the nature of the 16-dalton increase, the peptides of 827 and 819 *m/z* as well as 1141 and 1133 *m/z* were analyzed with a high resolution Orbitrap mass spectrometer. The difference between both the larger and the smaller pairs was 15.995 dalton, considered to be derived exclusively from the addition of one oxygen atom (Fig. 3, *A* and *B*). MS/MS revealed that the addition took place on the proline 565 and 530 residues (Fig. 3*C* and supplemental Fig. S5*A*). A 155.0808 *m/z* fragment observed in the high resolution MS/MS spectrum of the 819 *m/z* peak and a 171.0762 *m/z* fragment observed in the spectrum of the 827 *m/z* peak led to the exclusive identification of their chemical formulas as $C_7H_{11}O_2N_2$ and $C_7H_{11}O_3N_2$, respectively (Fig. 3*D*). Formulas $C_7H_{11}O_3N_2$ and $C_7H_{11}O_2N_2$ match hydroxyproline-glycine and unmodified proline-glycine, respectively.

Detection of Prolyl 4-Hydroxylation of α-Fibrinogen—The physiologically stable oxidation of proline occurs exclusively at the carbon in the fourth position (supplemental Fig. S5*B*). We used *Ganp* (germinal center-associated nuclear protein) (27) transgenic mice to produce a monoclonal antibody (named 11A5) that reacts with a synthetic peptide ESSSHHP(O)-GIAEFPSR (P(O), 4-hydroxyproline) (named HyP-ESS) but not with an unmodified synthetic peptide with the same amino acid sequence (ESS) (supplemental Fig. S6*A*). GANP mice can produce highly diverse antibodies and have been used with success to generate high affinity antibodies to various difficult antigens (18). We were unable to produce a monoclonal antibody with specificity for TFP(O)GFFSPMLGEFVSETESR (data not shown). Fibrinogen α-polypeptide is produced and secreted mainly by the liver. α-Fibrinogen with hydroxylation of its proline 565 residue (hereafter, αFG-565HyP) as well as 3 polypeptides (the α-, β-, and γ-chains) of fibrinogen were detected in the lysates (Fig. 4*A*) and supernatants (data not shown) of cultured hepatic cells and several hepatocellular carcinoma cell lines by immunoblotting with 11A5 monoclonal antibody. The 4-hydroxylation of proline is catalyzed by two types of enzymes: collagen-type and HIF1-type prolyl 4-hydroxylases (12, 28, 29). There are 4 collagen-type (*P4HA1*, *P4HA2*, *P4HA3*, and *P4HB*) and 3 HIF1-type (*EGNL1*, *EGNL2*, and *EGNL3*) prolyl 4-hydroxylase genes annotated in the human genome, but only knockdown of *P4HA1* by siRNA inhibited the production of αFG-565HyP by KIM-1 cells (Fig. 4*B* and supplemental Fig. S7*A*), indicating the involvement of P4HA1 (EC 1.14.11.2) in the 4-hydroxylation of the proline 565 residue of α-fibrinogen, at least in this cell line.

Prolyl 4-Hydroxylated α-Fibrinogen in Clinical Samples—The plasma level of αFG-565HyP was increased in pancreatic

FIGURE 1. **Representative MS peak with significant difference between pancreatic cancer patients and controls.** *A*, representative two-dimensional display of the entire set (>110,000) of MS peaks detected by 2DICAL with *m/z* values along the *x*-axis and retention time along the *y*-axis. *B*, peak at 552 *m/z* and 8.3 min displayed in various combinations of axes. Pancreatic cancer patients (*Case*) indicated in *red* and controls (*Control*) *blue*. *Upper left*, *m/z* and intensity axes with the indication of isotopic mass (*light blue line* and *dot*). *Lower left*, gray-scale intensity pattern of retention time (*x* axis) and sample (*y* axis). *Upper right*, sample and intensity axes (*left*) and a *box-and-whisker diagram* of pancreatic cancer patients and controls (*right*). *Lower right*, *m/z* and retention time axes with high (*upper*) and low (*lower*) intensities indicated by a *red dot*.

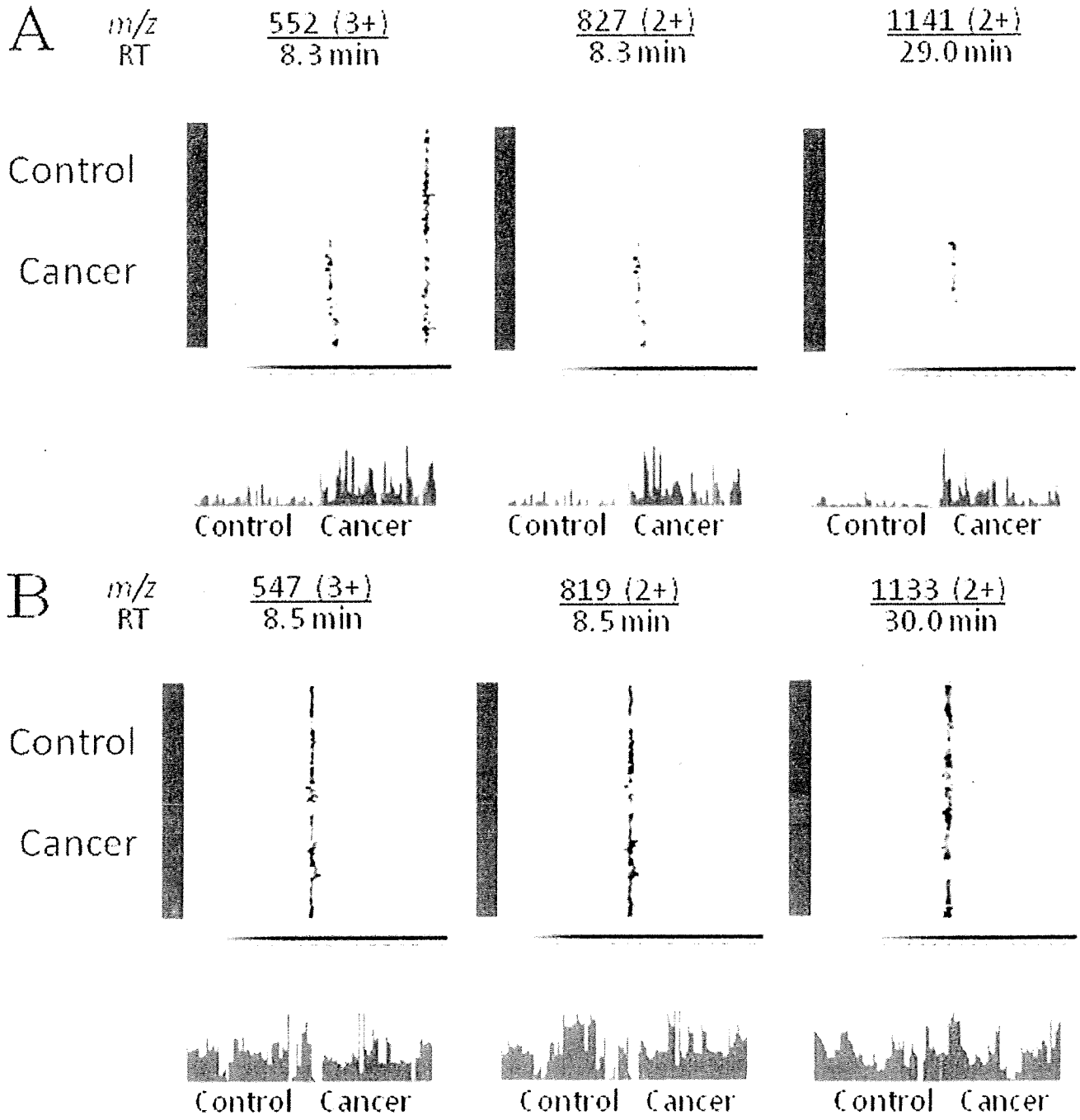

FIGURE 2. **Modified and unmodified peptide fragments with the same amino acid sequences.** *A*, peaks at 552, 827, 1141 *m/z* with significant difference between pancreatic cancer patients and controls. The axes are retention time and sample (*top*) and sample and intensity (*bottom*). *B*, peaks at 547, 819, and 1133 *m/z* matched to the above peaks of peptide fragment without modification.

cancer patients, but the levels of α-, β-, and γ-fibrinogen did not show any differences between pancreatic cancer patients and healthy controls (Fig. 4*C*). The levels of αFG-565HyP and α-fibrinogen were not significantly correlated (CC = 0.22) (supplemental Fig. S6, *B* and *C*). There was a significant correlation (CC = 0.81) between the intensity of the 827 *m/z* peak detected by 2DICAL and the level of αFG-565HyP determined by immunoblotting with 11A5 antibody (supplemental Fig. S7*B*), indicating the quantitative accuracy of 2DICAL. A competitive ELISA utilizing anti-HyP-ESS (11A5) monoclonal antibody was constructed (supplemental Fig. S6*D*), and the plasma level of αFG-565HyP was quantified in 685 individuals (Set 4) (Fig. 5). The plasma samples were collected prospectively from 7 medical institutions to ensure the absence of bias during the process of sample preparation. The ELISA assay showed high reproducibility with a median CV value of 0.079 among triplicates. There was a significant difference ($p = 3.80 \times 10^{-15}$, Mann-Whitney *U* test) in the plasma level of αFG-565HyP between 160 pan-

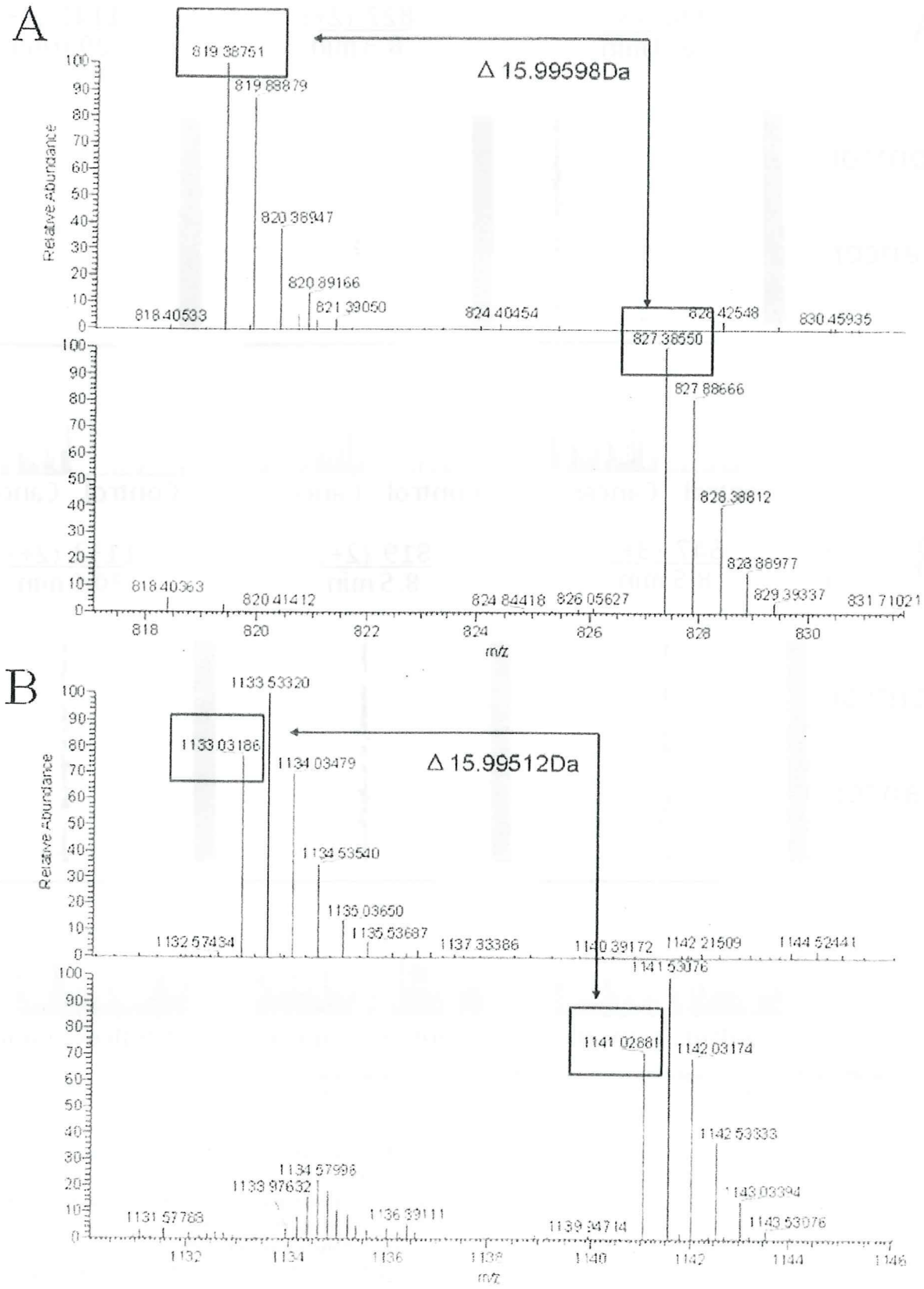

FIGURE 3. **Determination of the 16-dalton increase by high resolution MS.** *A* and *B*, high resolution MS spectra of the 827 and 819 *m/z* peaks (*A*) as well as the 1141 and 1133 *m/z* peaks (*B*) obtained with an Orbitrap mass spectrometer. *C*, MS/MS spectra of the 827, 1141, 819, and 1133 *m/z* peaks. *D*, 155.0808 *m/z* and 171.0762 *m/z* fragments exclusively identified as $C_7H_{11}O_2N_2$ and $C_7H_{11}O_3N_2$ with 5 ppm mass tolerance.

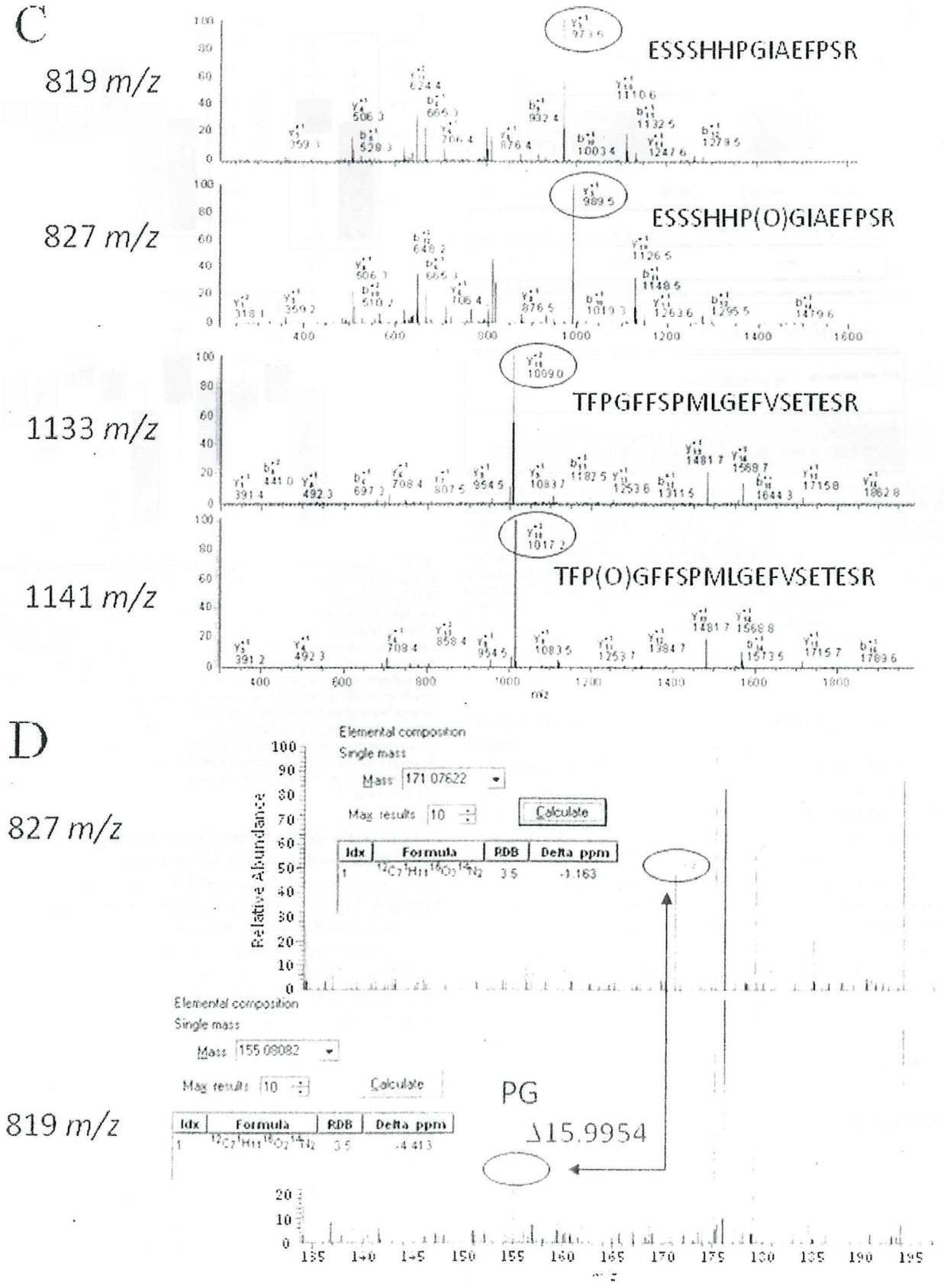

FIGURE 3—*continued*

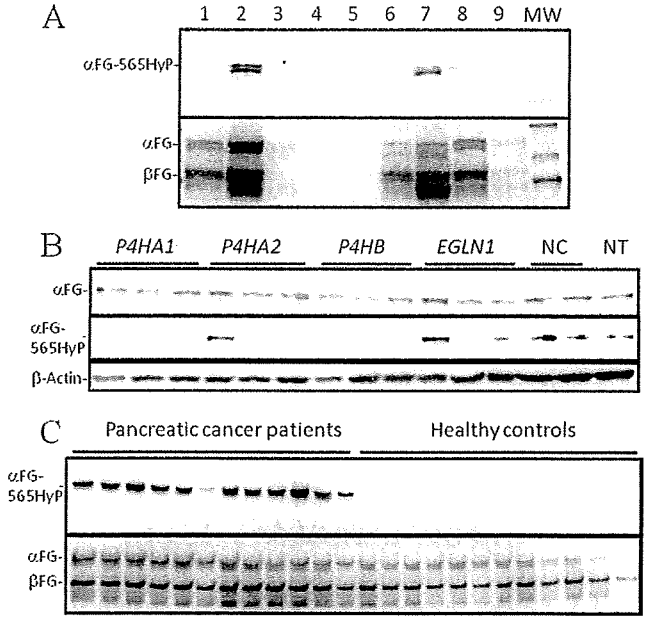

FIGURE 4. **Detection of prolyl 4-hydroxylated α-fibrinogen by immunoblotting.** *A*, lysates of normal hepatic cells (*lane 1*) and hepatocellular carcinoma KIM-1 (*lane 2*), Hep-3B (*lane 3*), SK-Hep-1 (*lane 4*), HLE (*lane 5*), Jhh-7 (*lane 6*), Hep-G2 (*lane 7*), HuH-7 (*lane 8*), and HuH-6clone5 (*lane 9*) cells were separated by SDS-PAGE and immunoblotted with anti-HyP-ESS and anti-fibrinogen (*FG*) antibodies. *B*, expression of the indicated genes was knocked in KIM-1 cells down by siRNA treatment (3 siRNAs for each gene). Forty-eight hours after transfection, the cell lysates were analyzed by immunoblotting with anti-HyP-ESS, anti-fibrinogen, and anti-β-actin (loading control) antibodies. *NC*, negative control (non-targeting RNA); *NT*, not treated. *C*, immunoblot analysis of plasma samples from pancreatic cancer patients and controls with anti-HyP-ESS and anti-fibrinogen antibodies.

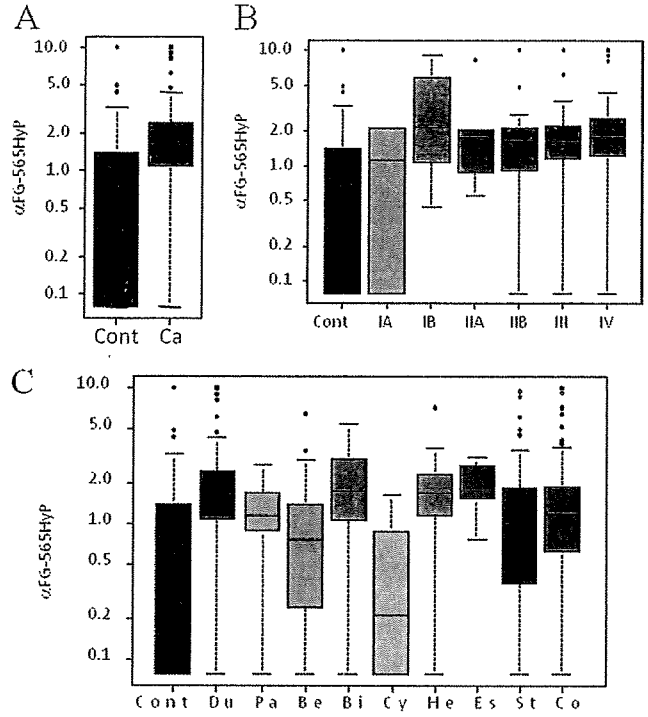

FIGURE 5. **Quantification of plasma prolyl 4-hydroxylated α-fibrinogen.** *A, box-and-whisker diagram* showing the different plasma levels of αFG-565Hyp in healthy controls (*Cont*, $n = 113$) and pancreatic cancer patients (*Ca*, $n = 160$). *Boxes* represent the median values and the 25–75 percentile range. *Whiskers* indicate the most extreme data point, which is no more than 1.5 times the interquartile range from the *boxes*. *B, box-and-whisker diagram* showing the plasma level of αFG-565Hyp in healthy controls (*Cont*, $n = 113$) and patients with stage-IA ($n = 2$), IB ($n = 4$), IIA ($n = 5$), IIB ($n = 28$), III ($n = 41$), and IV ($n = 78$) pancreatic cancer. *C, box-and-whisker diagram* showing the plasma level of αFG-565Hyp in healthy controls (*Cont*, $n = 113$) and patients with pancreatic ductal carcinoma (*Du*, $n = 160$), chronic pancreatitis (*Pa*, $n = 12$), benign pancreatic tumor or cyst (*Be*, $n = 37$), bile duct cancer (*Bi*, $n = 25$), cholecystitis (*Cy*, $n = 22$), hepatocellular carcinoma (*He*, $n = 14$), esophageal cancer (*Es*, $n = 10$), gastric cancer (*St*, $n = 147$), and colorectal cancer (*Co*, $n = 145$).

creatic cancer patients (2.26 ± 2.28 arbitrary units) and 113 healthy controls (0.91 ± 1.24) (Fig. 5*A*). The plasma level of αFG-565HyP was not elevated in patients with Stage IA (UICC, International Union Against Cancer) pancreatic cancer ($p = 0.811$), but patients with Stage IB or more advanced disease showed a significant increase of plasma αFG-565HyP ($p = 2.99 \times 10^{-2}$ to 1.88×10^{-12}) (Fig. 5*B* and supplemental Table S2). An elevated plasma level of αFG-565HyP was also observed in various cancers and chronic inflammatory disease. Patients with cancers of other organs (including the bile duct ($p = 4.24 \times 10^{-5}$), liver ($p = 1.08 \times 10^{-3}$), esophagus ($p = 2.07 \times 10^{-4}$), stomach ($p = 5.95 \times 10^{-4}$), and colon/rectum ($p = 9.29 \times 10^{-6}$)) as well as patients with chronic pancreatitis ($p = 3.89 \times 10^{-2}$) showed a significant increase in plasma αFG-565HyP (Fig. 5*C* and supplemental Table S3). Patients with benign pancreatic tumor/cyst ($p = 0.216$) or cholecystitis ($p = 0.111$) showed no significant difference from the controls.

DISCUSSION

Plasma proteomics by liquid chromatography and mass spectrometry (LC-MS) has been a challenge because of the complexity and individual diversity of human samples. We developed a simple but robust method that enables the quantitative comparison of multiple LC-MS data. In this study, we identified 6 MS peaks whose intensity was significantly different between 38 cancer patients and 39 healthy controls (Figs. 1 and 2 and supplemental Figs. S1 and S2) among a total of 115,325 peaks derived from Con A-binding plasma glycoproteins. High resolution MS/MS analysis revealed that 4 of 6 peaks were derived from prolyl 4-hydroxylated plasma α-fibrinogen (Fig. 3). Artificial oxidation of peptides/proteins frequently occurs during the preparative procedures for MS analysis, especially during separation by SDS-PAGE. However, the plasma samples from cancer patients and healthy controls used in this study were collected, stored, and processed in an identical manner and were not separated by SDS-PAGE. We deliberately validated the native hydroxylation of the proline residue of plasma α-fibrinogen by immunoblotting and ELISA with a modification-specific monoclonal antibody (Figs. 4 and 5).

Prolyl hydroxylation is essential for the folding, secretion, and stability of the collagen triple helix (28, 29). Collagen has long been considered to be the only protein that is hydroxylated on its proline residues, but recently the von Hippel Lindau (VHL) tumor suppressor gene product-mediated degradation of HIF1α was revealed to be regulated by prolyl hydroxylation (12). Prolyl 4-hydroxylation regulates the stability of argonaute 2 protein (13). However, it is largely unknown which other proteins are prolyl-hydroxylated and how the modification regulates the function of proteins. We found that the collagen-type

prolyl 4-hydroxylase P4HA1 is essential for the production of αFG-565HyP (Fig. 4*B*). Consistently, the consensus Xaa-Pro-Gly sequence of collagen (13, 30) was seen in the prolyl hydroxylation sites of α-fibrinogen (supplemental Fig. S5*A*). Prolyl-hydroxylated α-fibrinogen was produced in cultured hepatic cells and several hepatocellular carcinoma cell lines but not in pancreatic cancer cell lines (data not shown). Immunohistochemical study using antibody 11A5 showed that prolyl-hydroxylated α-fibrinogen existed at the inflammation site around the pancreatic cancer cells (data not shown). The modification change in plasma level may be determined by the production and consumption balance in the human body. Hydroxylation at proline 530 of α-fibrinogen was strongly correlated with αFG-565HyP (supplementary Fig. S7*C*). Multiple biological mechanisms may be involved in the regulation of prolyl-hydroxylated α-fibrinogen.

Post-translational modifications, such as glycosylation, phosphorylation, and oxidation, cause small differences in the molecular weight of proteins. Prolyl-hydroxylated peptides are 16 daltons larger than their unmodified counterparts, but this small change in molecular weight can readily be detected by 2DICAL as differences in the *m/z* values as well as the RT of the peptide peaks. The peaks derived from unmodified plasma fibrinogen fragments appeared in different locations (compare Fig. 2, *A* and *B*). Such modifications may be overlooked by MS/MS-based identification-oriented proteome approaches (31–34).

In this study, we were able to pinpoint the prolyl 4-hydroxylation of α-fibrinogen peptides in the large dataset of plasma samples (115,325 MS peaks × 231 LC-MS runs (77 cases in triplicate) = 27 million data points). Using a large independent validation cohort, newly constructed ELISA assay revealed the plasma level elevation of prolyl 4-hydroxylated α-fibrinogen in pancreatic cancer as well as other cancers and chronic inflammatory disease. Future studies will reveal the function of prolyl-hydroxylated α-fibrinogen and its regulation and clinical usage.

Acknowledgments—We thank Dr. Toshiaki Isobe, Dr. Hiroyuki Kaji (Tokyo Metropolitan University, Tokyo, Japan), and Dr. Hiroshi Nakayama (The Institute of Physical and Chemical Research (RIKEN), Wako, Japan) for suggestions on the interpretation of MS/MS data and Dr. Tomikazu Sasaki (University of Washington, Seattle, WA) for suggestions on prolyl hydroxylation. We also thank Dr. Masamichi Kojiro (Kurume University, Kurume, Japan) for provision of KIM-1 cells. We thank Ayako Igarashi, Tomoko Umaki, and Yuka Nakamura for excellent technical assistance and Daisuke Higo (Thermofisher Scientific, Tokyo, Japan) for Orbitrap mass spectrometry.

REFERENCES

1. Nedelkov, D., Kiernan, U. A., Niederkofler, E. E., Tubbs, K. A., and Nelson, R. W. (2005) *Proc. Natl. Acad. Sci. U.S.A.* **102,** 10852–10857
2. Ishihama, Y. (2005) *J. Chromatogr. A.* **1067,** 73–83
3. Takahashi, N., Kaji, H., Yanagida, M., Hayano, T., and Isobe, T. (2003) *J. Nutr.* **133,** 2090S–2096S
4. Gygi, S. P., Rist, B., Gerber, S. A., Turecek, F., Gelb, M. H., and Aebersold, R. (1999) *Nat. Biotechnol.* **17,** 994–999
5. DeSouza, L., Diehl, G., Rodrigues, M. J., Guo, J., Romaschin, A. D., Colgan, T. J., and Siu, K. W. (2005) *J. Proteome. Res,* **4,** 377–386
6. Ong, S. E., Blagoev, B., Kratchmarova, I., Kristensen, D. B., Steen, H., Pandey, A., and Mann, M. (2002) *Mol. Cell Proteomics* **1,** 376–386
7. Ono, M., Shitashige, M., Honda, K., Isobe, T., Kuwabara, H., Matsuzuki, H., Hirohashi, S., and Yamada, T. (2006) *Mol. Cell Proteomics* **5,** 1338–1347
8. Negishi, A., Ono, M., Handa, Y., Kato, H., Yamashita, K., Honda, K., Shitashige, M., Satow, R., Sakuma, T., Kuwabara, H., Omura, K., Hirohashi, S., and Yamada, T. (2009) *Cancer Sci.* **100,** 514–519
9. Matsubara, J., Ono, M., Negishi, A., Ueno, H., Okusaka, T., Furuse, J., Furuta, K., Sugiyama, E., Saito, Y., Kaniwa, N., Sawada, J., Honda, K., Sakuma, T., Chiba, T., Saijo, N., Hirohashi, S., and Yamada, T. (2009) *J. Clin. Oncol.* **27,** 2261–2268
10. Blombäck, B. (2001) *Ann. N. Y. Acad. Sci.* **936,** 1–10
11. Henschen-Edman, A. H. (2001) *Ann. N. Y. Acad. Sci.* **936,** 580–593
12. Jaakkola, P., Mole, D. R., Tian, Y. M., Wilson, M. I., Gielbert, J., Gaskell, S. J., Kriegsheim, Av., Hebestreit, H. F., Mukherji, M., Schofield, C. J., Maxwell, P. H., Pugh, C. W., and Ratcliffe, P. J. (2001) *Science* **292,** 468–472
13. Qi, H. H., Ongusaha, P. P., Myllyharju, J., Cheng, D., Pakkanen, O., Shi, Y., Lee, S. W., and Peng, J. (2008) *Nature* **455,** 421–424
14. Henschen, A. H., Theodor, I., and Pirkle, H. (1991) *Thrombosis Haemostasis* **65,** 821
15. Honda, K., Hayashida, Y., Umaki, T., Okusaka, T., Kosuge, T., Kikuchi, S., Endo, M., Tsuchida, A., Aoki, T., Itoi, T., Moriyasu, F., Hirohashi, S., and Yamada, T. (2005) *Cancer Res.* **65,** 10613–10622
16. Shitashige, M., Satow, R., Honda, K., Ono, M., Hirohashi, S., and Yamada, T. (2008) *Gastroenterology* **134,** 1961–1971, 1971.e1–4
17. Huang, L., Shitashige, M., Satow, R., Honda, K., Ono, M., Yun, J., Tomida, A., Tsuruo, T., Hirohashi, S., and Yamada, T. (2007) *Gastroenterology* **133,** 1569–1578
18. Sakaguchi, N., Kimura, T., Matsushita, S., Fujimura, S., Shibata, J., Araki, M., Sakamoto, T., Minoda, C., and Kuwahara, K. (2005) *J. Immunol.* **174,** 4485–4494
19. Harlow, E., and Lane, D. (1988) *Antibodies. A Laboratory Manual,* Cold Spring Harbor Laboratory, Cold Spring Harbor, NY
20. Sato, S., Idogawa, M., Honda, K., Fujii, G., Kawashima, H., Takekuma, K., Hoshika, A., Hirohashi, S., and Yamada, T. (2005) *Gastroenterology* **129,** 1225–1236
21. Ogata, S., Muramatsu, T., and Kobata, A. (1975) *J. Biochem.* **78,** 687–696
22. Zhang, H., Yi, E. C., Li, X. J., Mallick, P., Kelly-Spratt, K. S., Masselon, C. D., Camp, D. G., 2nd, Smith, R. D., Kemp, C. J., and Aebersold, R. (2005) *Mol. Cell. Proteomics.* **4,** 144–155
23. Hakomori, S. (1989) *Adv. Cancer Res.* **52,** 257–331
24. Ono, M., and Hakomori, S. (2004) *Glycoconj. J.* **20,** 71–78
25. Kumamoto, K., Mitsuoka, C., Izawa, M., Kimura, N., Otsubo, N., Ishida, H., Kiso, M., Yamada, T., Hirohashi, S., and Kannagi, R. (1998) *Biochem. Biophys. Res. Commun.* **247,** 514–517
26. States, D. J., Omenn, G. S., Blackwell, T. W., Fermin, D., Eng, J., Speicher, D. W., and Hanash, S. M. (2006) *Nat. Biotechnol.* **24,** 333–338
27. Kuwahara, K., Yoshida, M., Kondo, E., Sakata, A., Watanabe, Y., Abe, E., Kouno, Y., Tomiyasu, S., Fujimura, S., Tokuhisa, T., Kimura, H., Ezaki, T., and Sakaguchi, N. (2000) *Blood* **95,** 2321–2328
28. Myllyharju, J. (2003) *Matrix Biol.* **22,** 15–24
29. Kukkola, L., Hieta, R., Kivirikko, K. I., and Myllyharju, J. (2003) *J. Biol. Chem.* **278,** 47685–47693
30. Myllyharju, J., and Kivirikko, K. I. (1999) *EMBO J.* **18,** 306–312
31. Gao, J., Opiteck, G. J., Friedrichs, M. S., Dongre, A. R., and Hefta, S. A. (2003) *J. Proteome. Res.* **2,** 643–649
32. Liu, H., Sadygov, R. G., and Yates, J. R., 3rd (2004) *Anal. Chem.* **76,** 4193–4201
33. Ishihama, Y., Oda, Y., Tabata, T., Sato, T., Nagasu, T., Rappsilber, J., and Mann, M. (2005) *Mol. Cell Proteomics.* **4,** 1265–1272
34. Mueller, L. N., Brusniak, M. Y., Mani, D. R., and Aebersold, R. (2008) *J. Proteome. Res.* **7,** 51–61

Oncogene (2009) 28, 2903–2909

www.nature.com/onc

ORIGINAL ARTICLE

Significance of RRM1 and ERCC1 expression in resectable pancreatic adenocarcinoma

H Akita[1], Z Zheng[2], Y Takeda[1], C Kim[1], N Kittaka[1], S Kobayashi[1], S Marubashi[1], I Takemasa[1], H Nagano[1], K Dono[1], S Nakamori[3], M Monden[1], M Mori[1], Y Doki[1] and G Bepler[2]

[1]Department of Surgery, Osaka University Graduate School of Medicine, Osaka, Japan; [2]Department of Thoracic Oncology, H. Lee Moffitt Cancer Center and Research Institute, University of South Florida, Tampa, FL, USA and [3]Department of Surgery, National Hospital Organization Osaka National Hospital, Osaka, Japan

The identification of molecular markers, useful for therapeutic decisions in pancreatic cancer patients, is crucial for advances in disease management. Gemcitabine, although a cornerstone of current therapy, has limited efficacy. *RRM1* is a key molecule for gemcitabine efficacy and is also involved in tumor progression. We determined *in situ* *RRM1* and *excision repair cross complementation group 1* (*ERCC1*) protein levels in 68 pancreatic cancer patients. All had R0 resections without preoperative therapy. Protein levels were determined by automated quantitative analysis (AQUA), a fluorescence-based immunohistochemical method. The relationship between protein expressions and clinical outcomes, including response to gemcitabine at the time of disease recurrence, was determined. Patients with high *RRM1* showed significantly better overall survival than patients with low expression ($P=0.0196$). There was a trend toward better overall survival for patient with high ERCC1 ($P=0.0552$). When both markers were considered together, patients with both high *RRM1* and *ERCC1* faired the best in terms of overall and disease-free survival ($P=0.0066$, $P=0.0127$). In addition, treatment benefit from gemcitabine in patients with disease recurrence was observed only in patients with low *RRM1*. The combination of *RRM1* and *ERCC1* expression is prognostic in pancreatic cancer patients after a complete resection. On disease recurrence, only patients with low *RRM1* derive benefit from gemcitabine.
Oncogene (2009) **28,** 2903–2909; doi:10.1038/onc.2009.158; published online 22 June 2009

Keywords: pancreatic cancer; *RRM1*; *ERCC1*; AQUA; prognosis; gemcitabine

Introduction

Pancreatic cancer is one of the leading causes of tumor-related mortalities. The prognosis of patients after complete resection is poor, and more than 50% of patients develop tumor recurrence at distant or locoregional sites, with an estimated 5-year survival of only 20% (Kayahara *et al.*, 1993; Nitecki *et al.*, 1995; Staley *et al.*, 1996; Sener *et al.*, 1999; Li *et al.*, 2004). The addition of chemotherapy and radiotherapy to surgical resection is important, and gemcitabine, a pyrimidine nucleotide analogue, has become the standard chemotherapeutic agent in such programs (Burris *et al.*, 1997; Oettle *et al.*, 2007) (Rothenberg *et al.*, 1996). However, the clinical response rate to gemcitabine remains modest, mainly because of the profound chemoresistance inherent in pancreatic cancer. The selection of patients who derive a true benefit from gemcitabine could be an important stepping stone toward improvement of outcome of pancreatic cancer.

RRM1, the gene that encodes the regulatory subunit of ribonucleotide reductase, is a key determinant of gemcitabine efficacy. In various cancers, we and others have described that overexpression of the *RRM1* gene is strongly associated with gemcitabine resistance (Cao *et al.*, 2003; Rosell *et al.*, 2004; Bergman *et al.*, 2005; Bepler *et al.*, 2006; Nakahira *et al.*, 2007). However, there is no clinical study that investigated the correlation between *RRM1* protein expression and gemcitabine resistance.

On the other hand, the expression of *RRM1* was also reported to correlate with the tumorigenic and metastatic potential of lung cancer (Gautam *et al.*, 2003), and an oncogenic ras-transformed cell line with high expression of an *RRM1* transgene had reduced metastatic potential (Fan *et al.*, 1997). Furthermore, high expression of *RRM1* in transgenic mice is associated with resistance to carcinogen-induced lung tumorigenesis (Gautam and Bepler, 2006). Recently, overexpression of *RRM1* and the *excision repair cross-complementation group 1* (*ERCC1*) gene product was reported to correlate with favorable prognosis in non-small-cell lung cancer (Zheng *et al.*, 2007).

The present study was designed to evaluate the protein expression of *RRM1* and *ERCC1* in pancreatic cancer by automated quantitative analysis (AQUA). We describe the relationship between *RRM1* and *ERCC1* expression, the association between the expression of these proteins and prognosis, as well as the response to

Correspondence: Dr Y Takeda, Department of Surgery, Osaka University Graduate School of Medicine, 2-2, Yamadaoka, Suita-city, Osaka 5650871, Japan.
E-mail: ytakeda@gesurg.med.osaka-u.ac.jp
Received 24 November 2008; revised 23 March 2009; accepted 14 May 2009; published online 22 June 2009

gemcitabine therapy. To our knowledge, this study is the first to examine both the prognostic and predictive aspects of *RRM1* in the same clinical samples.

Results

RRM1 and ERCC1 expression characteristics

We constructed a tissue microarray using triplicate 0.6-mm cores from formalin-fixed and paraffin-embedded specimens of the primary tumor. Immunostaining showed a granular nuclear pattern for *RRM1*, and a fine granular pattern for *ERCC1* (Figure 1). Next, we used AQUA to analyse the expression levels of *RRM1* and *ERCC1* in specimens obtained from 68 patients. The scores of *RRM1* ranged from 116 to 1644 (median, 539; mean, 546) for all specimens, and the scores of *ERCC1* ranged from 55 to 1469 (median 382, mean 412).

The average score of triplicate tissues from each patient was used for analysis of the association between staining and clinical parameters. The AQUA scores for *RRM1* did not correlate significantly with those of *ERCC1* ($r=0.172$, $P=0.1610$) (Figure 2). The median values of *RRM1* and *ERCC1* expression levels were used to divide the patients into high and low expression groups. There were no significant differences between patients with high and low tumoral *RRM1* expression or high and low tumoral *ERCC1* expression with respect to age, sex, histopathological type (well/mod/poor), tumor size, tumor location (head/body/tail), pathological depth of tumor (pT1/T2/T3), the total number of resected lymph nodes, pathological lymph node metastasis (negative/positive) and the number of metastatic

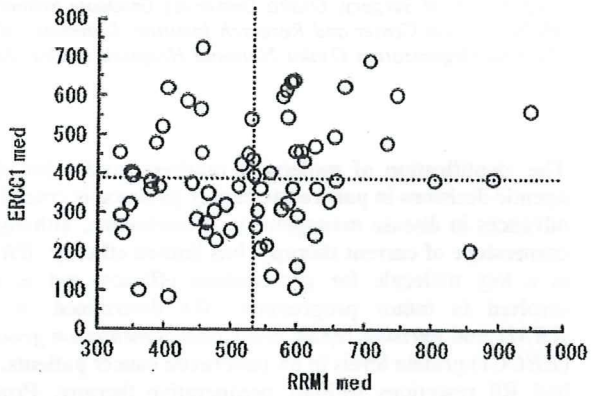

Figure 2 Relationship between automated quantitative analysis (AQUA) scores of *RRM1* and *excision repair cross-complementation group 1* (*ERCC1*) expression. *RRM1* expression did not correlate with that of *ERCC1* ($r=0.172$, $P=0.161$).

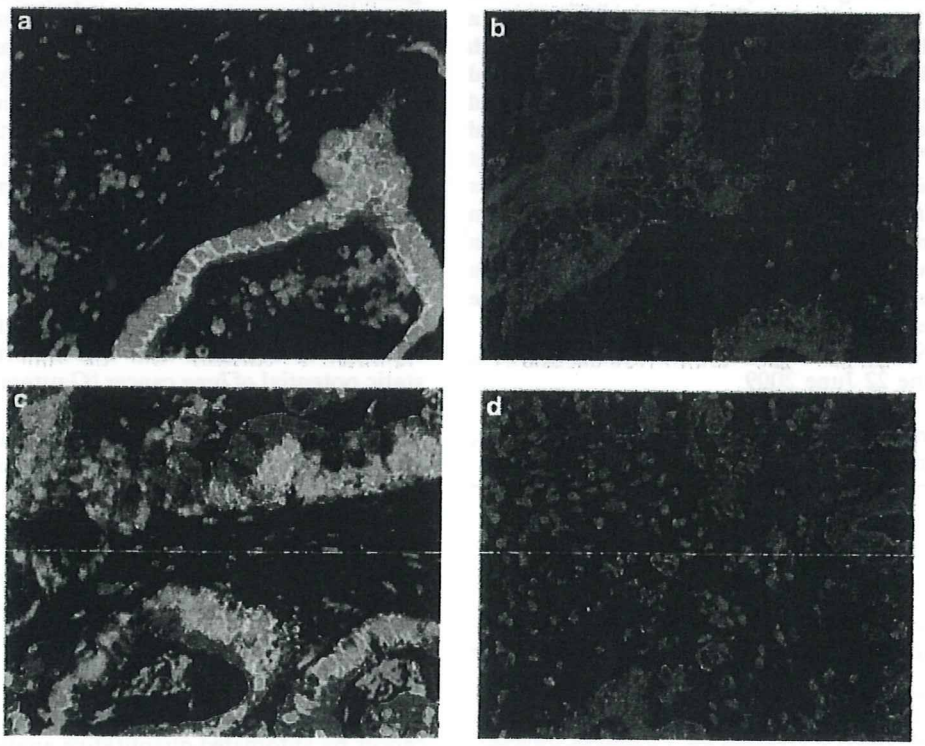

Figure 1 Staining for *RRM1* and *excision repair cross-complementation group 1* (*ERCC1*) proteins. (**a**) *RRM1*-positive sample. Note the granular nuclear pattern. Nucleus, blue; cytoplasm, red; *RRM1*, green; and merged, light blue to light green. (**b**) *RRM1*-negative sample. Nucleus, blue; and cytoplasm, red. (**c**) *ERCC1*-positive sample. Note the fine granular pattern in the nucleus. Nucleus, blue; cytoplasm, red; *ERCC1*, green; and merged, light blue to light green. (**d**) *ERCC1*-negative sample. Nucleus, blue; and cytoplasm, red.

Table 1 Relationship between protein expression levels and clinicopathological factors

	RRM1 expression level			*ERCC1 expression level*		
	High	*Low*	P-*value*	*High*	*Low*	P-*value*
Age (years) (mean ± s.d.)	66.8 ± 7.6	64.4 ± 7.9	0.220	64.6 ± 7.7	66.6 ± 7.8	0.283
Sex (male/female)	15/19	18/16	0.628	15/19	18/16	0.628
Histopathology (well/mod/poor)	17/14/3	9/18/7	0.102	12/19/3	14/13/7	0.237
Tumor size (cm) (mean ± s.d.)	27.4 ± 9.3	26.7 ± 8.2	0.752	25.2 ± 8.2	28.9 ± 8.9	0.077
Tumor location (head/body/tail)	27/6/1	27/4/3	0.497	27/4/3	27/6/1	0.497
pT (T1/T2/T3)	1/1/32	1/0/33	0.602	1/1/32	1/0/33	0.602
Total number of resected lymph node	34.4 ± 12.9	30.3 ± 13.6	0.243	30.8 ± 10.6	34.3 ± 15.7	0.330
PN (positive/negative)	12/22	17/17	0.327	18/16	11/23	0.141
Total number of metastatic lymph node	1.6 ± 1.9	1.0 ± 1.7	0.202	1.1 ± 1.7	1.5 ± 1.9	0.315
Gem therapy (+/−)	14/20	14/20	0.999	13/21	15/19	0.806

Abbreviation: *ERCC1, excision repair cross-complementation group 1.*

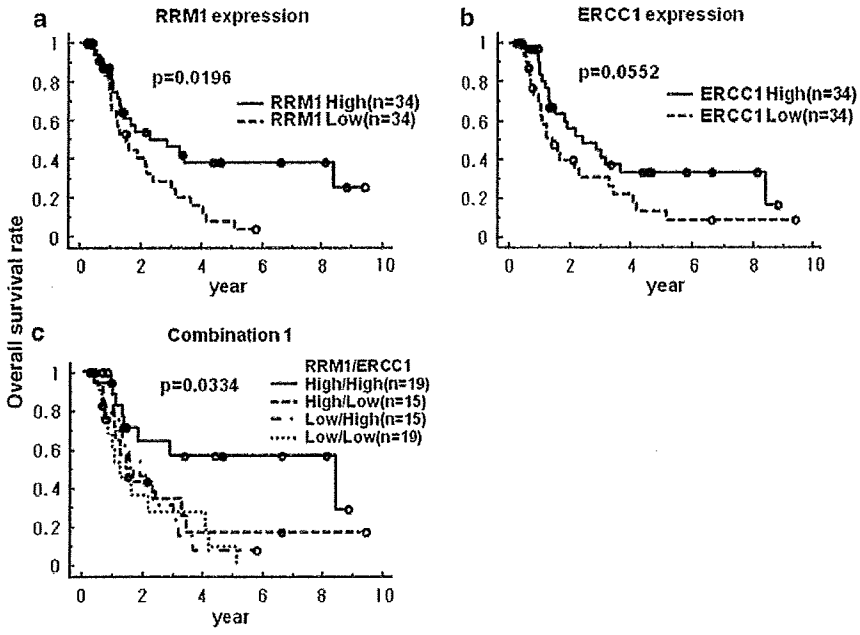

Figure 3 Relationship between *RRM1* and *excision repair cross-complementation group 1* (*ERCC1*) expression levels and overall survival rate. (a) Relationship between *RRM1* and overall survival is significant (3-year survival; 46.3 versus 28.6%, $P=0.0196$). (b) Relationship between *ERCC1* and overall survival is marginal ($P=0.0552$). (c) Relationship between the combination of *RRM1* and *ERCC1* expression levels in the same tumor and overall survival rate. Only high expression levels of *RRM1* and *ERCC1* in the same tumor related with the improvement of overall survival rate ($P=0.0334$).

lymph nodes, and whether or not gemcitabine was used as chemotherapy (Table 1).

Relationship between RRM1/ERCC1 expression and prognosis

The median overall survival of all patients was 16.3 months (4.3–113) and the median disease-free survival was 10.3 months (2–106). The Kaplan–Meier overall survival estimates were significantly better for patients with high *RRM1* expression compared with those having low *RRM1* expression levels (3-year survival; 46.3 versus 28.6%, $P=0.0196$) (Figure 3a). Likewise, patients with high *ERCC1* expression had a better overall survival than those with low levels of expression; although this difference was only marginally significant ($P=0.0552$) (Figure 3b). When we divided the 68 patients into four groups; that is, high tumoral expression of both proteins (High/High, $n=19$), high expression of only *RRM1* (High/Low, $n=15$), high expression of only *ERCC1* (Low/High, $n=15$) and low expression of both proteins (Low/Low, $n=19$); only patients of the High/High group had a significantly better prognosis than the others (3-year survival; 56.7 versus 30.5%, $P=0.0066$) (Figure 3c, Supplementary Figure 1).

With regard to disease-free survival, high *ERCC1* expression levels were significantly associated with better outcome (3-year survival; 30.2% for high versus

23.1% for low, $P=0.0454$). There was no significant difference in disease-free survival between the high and low *RRM1* expression groups (Supplementary Figures 2A and B). With respect to the combination of *RRM1* and *ERCC1*, only the High/High group showed a significantly better disease-free survival compared with the other groups (3-year survival, 43.2 versus 19.2%, $P=0.0127$) (Supplementary Figures 2C and D).

Univariate and multivariate analysis of factors associated with prognosis

We investigated the prognostic significance of various clinicopathological factors in pancreatic cancer patients who underwent radical resection. Univariate analysis showed that only the pathological type and absence or presence of lymph node metastases, were prognostically significant for disease-free survival ($P=0.034$, 0.025, respectively), and both parameters had marginal significance for overall survival ($P=0.078$, 0.084, respectively) (Table 2). Multivariate analysis identified the *RRM1* expression level as the only independent determinant of overall survival (hazard ratio (HR) 1.89, $P=0.046$), and none of the parameters tested was selected by the analysis as a significant prognostic factor in disease-free survival.

RRM1 expression and response to gemcitabine

Of all the 68 patients, 28 received therapy with single-agent gemcitabine. In 23 patients, this treatment was initiated at the time of tumor recurrence. To elucidate the relationship between *RRM1* expression level and gemcitabine therapy, we used survival after recurrence, which represented the period from starting gemcitabine therapy or other therapies in 50 patients with relapse, until death. First, we examined the survival benefit of gemcitabine. The 23 patients who were treated with gemcitabine had a significantly better survival than those who did not ($P=0.0074$) (Supplementary Figure 3). After dividing patients that were treated with gemcitabine into high and low *RRM1* expression groups, only patients with low *RRM1* expression benefited from gemcitabine therapy ($P=0.0010$) (Figure 4b). The survival of patients with high *RRM1* expression treated with gemcitabine was not significantly better than of those not treated with gemcitabine ($P=0.3309$) (Figure 4a). The interaction term between *RRM1* expression and gemcitabine treatment was significant for survival after recurrence ($P=0.0109$).

Discussion

Ribonucleotide reductase, composed of the regulatory subunit *RRM1* and the catalytic subunit *RRM2*, is a key enzyme involved in DNA synthesis, catalyzing the biosynthesis of deoxyribonucleotides from the corresponding ribonucleotides (Wright *et al.*, 1990; Hurta and Wright, 1992). *ERCC1*, a structure-specific DNA repair endonuclease responsible for the 5′ incision, has a key role in the removal of adducts from genomic DNA

Table 2 Prognostic factors for postoperative survival by Cox's proportional hazard model

	Univariate analysis				*Multivariate analysis*			
	DFS		*OS*		*DFS*		OS	
	HR	P-*value*	*HR*	P-*value*	*HR*	P-*value*	*HR*	P-*value*
Histology (poor, mod/well)	1.91	0.034	1.75	0.078	1.77	0.066	1.56	0.172
PN (positive/negative)	2.00	0.025	1.76	0.084	1.73	0.107	1.50	0.256
RRM1 expression (low/high)	1.55	0.129	2.04	0.022	1.39	0.265	1.89	0.046
ERCC1 expression (low/high)	1.75	0.048	1.78	0.059	1.42	0.265	1.54	0.194

Abbreviations: DFS, disease-free survival; *ERCC1*, excision repair cross-complementation group 1; HR, hazard ratio and OS, overall survival.

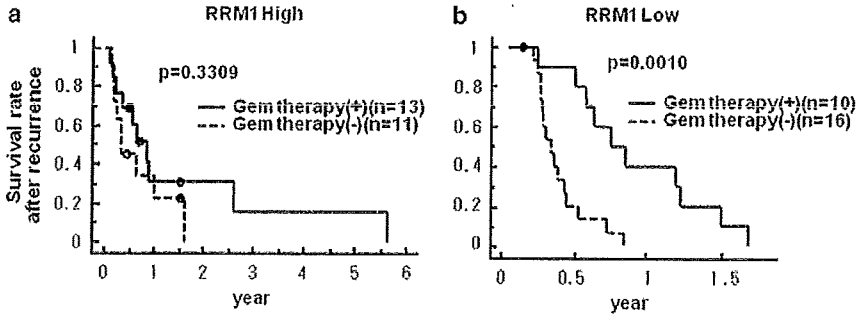

Figure 4 Relationship between survival after recurrence and patients treated with or without gemcitabine (**a**) in high *RRM1* expression group, and (**b**) in low expression group. Only patients with low *RRM1* expression benefited from gemcitabine therapy ($P=0.0010$).